Mechanics of Advanced Materials and Structures

ISSN: 1537-6494 (Print) 1537-6532 (Online) Journal homepage: https://www.tandfonline.com/loi/umcm20

Numerical and experimental procedure for material calibration using the serial/parallel mixing theory, to analyze different composite failure modes

Joel Jurado Granados, Xavier Martinez, Niamh Nash, Carlos Bachour, Ioannis Manolakis, Anthony Comer & Daniel Di Capua

To cite this article: Joel Jurado Granados, Xavier Martinez, Niamh Nash, Carlos Bachour, Ioannis Manolakis, Anthony Comer & Daniel Di Capua (2019): Numerical and experimental procedure for material calibration using the serial/parallel mixing theory, to analyze different composite failure modes, Mechanics of Advanced Materials and Structures, DOI: 10.1080/15376494.2019.1675106

To link to this article: https://doi.org/10.1080/15376494.2019.1675106

© 2019 The Author(s). Published with license by Taylor and Francis Group, LLC

Published online: 31 Oct 2019.

Submit your article to this journal

Article views: 921

View related articles

View Crossmark data

Full Terms & Conditions of access and use can be found at
https://www.tandfonline.com/action/journalInformation?journalCode=umcm20

MECHANICS OF ADVANCED MATERIALS AND STRUCTURES
https://doi.org/10.1080/15376494.2019.1675106

Taylor & Francis
Taylor & Francis Group

ORIGINAL ARTICLE

OPEN ACCESS Check for updates

Numerical and experimental procedure for material calibration using the serial/parallel mixing theory, to analyze different composite failure modes

Joel Jurado Granados[a], Xavier Martinez[a], Niamh Nash[b], Carlos Bachour[b], Ioannis Manolakis[b]*, Anthony Comer[b], and Daniel Di Capua[a]

[a]International Center for Numerical Methods in Engineering (CIMNE), Polytechnic University of Catalonia (UPC), Barcelona, Spain; [b]Irish Composites Centre (IComp), School of Engineering, Bernal Institute, University of Limerick, Limerick, Ireland

ABSTRACT

This work proposes a calibration procedure to obtain the material parameters required by the Serial/Parallel Mixing Theory for the analysis of composites. A set of experimental tests are defined to obtain the main composite failure modes. Then, it is proposed to calculate the parameters required by the formulation using the experimental results. The procedure proposed is validated by comparing the numerical results, with those obtained from the experimental campaign. This comparison shows that the Serial/Parallel mixing theory is capable of representing the failure modes of the composite for different loading scenarios as well as the material toughness.

ARTICLE HISTORY
Received 4 June 2019
Accepted 28 September 2019

KEYWORDS
Composites; serial/parallel mixing theory; calibration procedure; composite failure; composite toughness; experimental characterization; nonlinear performance

1. Introduction

Nowadays, the use of composite materials is extended to many engineering fields such as aeronautical, civil, naval, automotive, oil and gas and the energy industry. Consequently, a lot of research has been conducted to obtain new and better composites, improving the manufacturing processes or completing extensive test campaigns. This effort has contributed to building extensive databases of the properties and performance of composite materials, related to their static and fatigue behavior as well as their failure modes. Examples are the experimental campaigns conducted in the 90s for testing materials used in the wind turbine industry [1].

From the point of view of the design process, structural engineers are required to predict the performance of composite structures. Therefore, they need tools to help them to design reliable, safe and optimized solutions. One of these tools are numerical models, which are able to predict the mechanical behavior of composite materials, including their complex failure modes, such as delamination, fiber breakage or matrix cracking. However, the numerical models only by themselves are useless if the material properties are not well defined and obtained. As a consequence, they require a standardized calibration process. Composite laminates have different failure modes, which can interact between them, making their failure prediction difficult to capture. One of the reasons that explains their complex behavior is the microstructure of composites, i.e., laminates are made of stacked plies, with different orientations and each ply consists of two different materials which are embedded together. Hence, the interaction between the different plies, the individual behavior of each constituent material, and the interaction between the reinforcement and the matrix will govern the global performance of the whole composite. Considering these factors, a first approach to classify the failure modes of laminates can be performed.

The first failure group is defined by the interaction between different plies, and leads to one of most well-known failure modes of laminates, delamination. Delamination consists of a flat crack separating two adjacent plies, which prevents the transfer of shear load between the two plies. This failure usually appears due to poor interlayer bonding or interlayer strength [2, 3], due to an excessive shear stress in the laminate [4] or as a consequence of transverse cracks in the matrix that lead to delamination [5–7]. Finally, delamination causes a decrease of the laminate stiffness and a loss of effective strength in the material [3, 8, 9].

Another failure group can be defined by the failure of the constituent materials, which are the fiber and the matrix. Among these, the two most frequent failures are fiber breakage and matrix cracking. Many authors have observed fiber breakage as a failure mechanism in laminates loaded parallel to the fibers, such as Rosen *et al.* [10], Sanders *et al.* [11] and Daniel *et al.* [12]. Fiber breakage is related to the ultimate strength of the fibers, which are the load-bearing

CONTACT Joel Jurado Granados jjurado@cimne.upc.edu International Center for Numerical Methods in Engineering (CIMNE), C1 Building, Campus Nord, Polytechnic University of Catalonia (UPC), Gran Capita, s/n, Barcelona, 08034, Spain.
Color versions of one or more of the figures in the article can be found online at www.tandfonline.com/umcm.
*Present address: Department of Life Sciences, School of Science, Institute of Technology Sligo, Sligo, Ireland.

© 2019 The Author(s). Published with license by Taylor and Francis Group, LLC
This is an Open Access article distributed under the terms of the Creative Commons Attribution-NonCommercial-NoDerivatives License (http://creativecommons.org/licenses/by-nc-nd/4.0/), which permits non-commercial re-use, distribution, and reproduction in any medium, provided the original work is properly cited, and is not altered, transformed, or built upon in any way.

element of the laminate, leading to catastrophic failure of the laminate. This type of failure is observed in laminates in which at least one of the plies is loaded parallel to their fiber direction. Another failure mechanism is fiber buckling, which basically involves a lower compressive strength of the laminate compared to the tensile strength for those laminates loaded parallel to the fiber direction. This failure mode suggests that under bending loads, the first fibers that break are those under compressive stresses [13, 14]. Matrix cracking is related to matrix strength and can appear independently of the ply orientation, in the form of transverse cracks or cracks parallel to the fiber direction [15–17]. These cracks are usually the first sign of damage in the laminate [18], although it does not mean an imminent collapse of the structure. However, they can cause a reduction of laminate stiffness and can prompt other failure modes, such as delamination.

Finally, a new failure group can be defined which corresponds to the interface between the fiber and the matrix. The failure of this interface leads to a situation in which the loads are not transferred between constituent materials. Different performance can be observed depending on the strength of the interface [19]. If the interface bonding is weak, matrix cracks will grow easily and fiber pull-out will occur quite easily. On the other hand, a strong bond will delay the appearance of matrix cracks and lead to catastrophic failure caused by fiber fracture.

Throughout the history of composites, different models have been developed to predict their mechanical performance. A first approach consists of analyzing the composite at laminate level, e.g., Classical Laminate Theory (CLT), which assumes that the deformation of the lamina can be obtained from the deformation of its mid-plane and its curvature, without variations in its thickness direction [20]. This method is able to predict displacements, strains and stresses, assuming thin laminates and elastic materials. The main advantage of the model is simplicity, it can account for the anisotropic properties of the laminate, and it can be coupled with different failure criteria. These failure criteria are based on relations between several parameters at a ply level, such as strains or stresses. Among the most well-known failure criteria are maximum stress/strain criteria and quadratic Tsai-Hill and Tsai-Wu. A review of these theories can be found in the literature [21]. The recent research on the development of failure criteria leads to the improvement of the traditional methods and to evaluate them for new material systems. For instance, Gu *et al.* [22] applied some modifications to Hashin's failure criteria for UD composite materials, who modified tensile fiber mode and tensile matrix mode, based on physical considerations. Chen *et al.* [23] focused on establishing a unified theory of yield and failure criteria to predict the inter-fiber failure, considering the effect of normal stress on the shear strength by introducing a coupling term. Koh *et al.* [24] analyzed four common failure criteria, in order to understand how well they predict strength in multidirectional flax fiber composite laminates. Although many failure criteria can take into account some interaction between different failure mechanisms, e.g., Tsai-Hill and Tsai-Wu, they have several drawbacks. The most relevant drawbacks are that some of the strength values required by the model need to be adjusted for a specific ply thickness and/or composite configuration. In addition, there is no information about the damage progression in the laminate. Therefore, for composite structures, the use of a failure criterion is not always enough to obtain the failure mechanism and the final collapse load of the structure. This is the main reason why other approaches have been developed.

Instead of defining a failure threshold, it is possible to use non-linear constitutive models based on thermodynamic principles, to obtain the performance of the composite. For example, Maimi *et al.* [25, 26] proposed a continuum mechanics model to account for different lamina failure modes, which is based on the LARC models previously developed by Camanho, Davila and other authors [27, 28]. In addition, a fracture mechanics approach is used in order to follow the evolution of several failure modes in composites, such as delamination or crack densities [29]. Ladevèze *et al.* [30], proposed to model a single layer and interface as two meso-constituents and assumed that the fracture of the material is only described by means of delamination and through-thickness cracks. Matzenmiller *et al.* [31] introduced internal variables to describe the evolution of the damage state, using a thermodynamic approach. Williams *et al.* [32] used plane-stress continuum damage mechanics to predict impact damage growth. Barbero *et al.* [33, 34] presented a model based on a combination of two constituent-level models and an interphase model, decomposing the state variables by micromechanics. The research line is still open and prove of it are the work done by several recent authors. Such as Skovsgaard *et al.* [35, 36], who proposed a three-dimensional constitutive model able to predict strain localization of composites, including kink band formation, The model is based on constitutive relations for the constituents and is formulated using nominal stress rates and velocity gradients, which implies that can be used in finite strain regime. O'Shea *et al.* [37] used a strain energy function capable of modeling compressible orthotropic materials under large deformations. O'Shea validated the formulation through analysis of single family fiber-reinforced composites and biological tissues under large tensile and shear deformations. Staber *et al.* [38] also developed a hyper-elastic model for composites but using a stochastic approach. Staber used a two-steps approach for the calibration strategy, where on the first one the linearized model is considered in order to obtain the mean values. In the second step, the principal component analysis is combined with the maximum method to estimate the dispersion parameter and the correlation lengths. A different approach is based on obtaining the composite performance by means of its constituent materials. This approach has the advantage of taking into account different phenomena related to constituent materials and obtaining a more realistic outcome, given that composites are heterogeneous materials. Following this approach, there are two models that are worthy of mention: numerical multi-scale models and the use of the Rule of Mixtures as a

constitutive law manager. Both are described in the following.

Multi-scales models define a two-scale context: global scale and micro-scale. The global scale, or macroscale, solves the global response of the composite structure, considering the composite as a homogenous material. The micro-scale is solved on a Representative Volume Element (RVE) which is defined to characterize the internal micro-structure of the composite. The main advantage of this approach is that it takes into account all micro-structural phenomena and material interactions that occur in the composite, for instance fiber-matrix debonding, fiber buckling, fiber kink-band formation, matrix degradation, thermal effects, and performance of woven-type composites, among others. Nevertheless, multi-scale models are extremely costly in terms of computational time and memory, making the study of complex composite structures almost unaffordable. The use of multi-scale procedures for the analysis of composite materials is found in the work of Otero *et al.* [39] who presented a two-scale homogenization procedure to analyze three dimension composite structures. Chen *et al.* [40] proposed a viscoelastic model for fiber-reinforced composites undergoing finite deformations, in a homogenization framework. Representative volume element (RVE) models for unit cells of the composite were used to perform numerical simulations based on the proposed constitutive model. Liu *et al.* [41] used the mechanics of structure genome (MSG) as a multi-scale and multi-physics approach for constitutive modeling of composite structures, with the aim of capture the pointwise temperature load on weave laminates. As has been previously stated, and it is proved in [42]), one of the main drawbacks of multi-scale procedures is their computational cost. For this reason, several efforts have been made to reduce the computational requirements of these analysis, especially when the material becomes non-linear. With this purpose, Otero *et al.* [43] developed a non-linear strategy to minimize the times in which the RVE has to be analyzed, and Zaghi *et al.* [44] proposed the construction of a discrete constitutive law based on an off-line analysis of the RVE.

The Classical Rule of Mixtures (RoM) was initially proposed by Trusdin and Toupin [45]. It obtains the composite performance by the sum of the contributions of each constituent material, proportionally to their volumetric participation. Car *et al.* [46, 47] used the classic RoM of Trusdell and Toupin and applied a thermodynamic approach, treating the classical RoM as a constitutive law manager, and hence taking into account the non-linear performance of the composite by means of the non-linear behavior of the constituent materials. Later, Rastellini *et al.* [48] obtained a more realistic formulation, named Serial/Parallel Mixing Theory (S/P RoM). The main advantages of S/P RoM are that the model takes into account the anisotropic behavior of laminates, and therefore materials can be simulated with any constitutive equation and many failure modes of the composite can be predicted. The formulation is designed to take into account the anisotropy of laminates, independently of the fiber volume content or fiber orientation. Hence, once the fiber and matrix characterization is made, the formulation can obtain the non-linear performance of any composite material, regarding its loading direction, stacking sequence or fiber content, which reduces the number of tests to be done to obtain the laminate mechanical properties. The validity of the S/P RoM to accurately characterize different composite failure modes has been already proved in several publications. Initial analyses where focused in the characterization of fiber and matrix failure [48]. Afterwards, the formulation has been used to predict composite delamination [49, 50], and delamination after impact [51], in [14] the formulation is enhanced to simulate fiber buckling. And, more recently, it has proved its capacity to predict the failure due to compression around composite holes [52]. Another feature of this formulation that gives a clear advantage compared with multi-scale models is its computational cost. S/P RoM solves the laminate and constituents equations at each Gauss point, and hence, solving a micro-model is not required to obtain the non-linear performance. Given the capability of S/P RoM to predict different failure modes for composites by only analyzing the failure modes of their components and its lower computational cost compared with other models, the Serial/Parallel Mixing Theory approach is the one followed and described in this work.

Any model developed to characterize any given material performance requires some material parameters that must be calibrated. In the case of composites, these parameters are usually obtained from testing data, which can be conducted at laminate, lamina or constituent levels. Some authors such as Ribeiro *et al.* [53] and Barbero *et al.* [54, 55] have developed their own processes. On the one hand, Ribeiro's method consists of the definition of several laminate tests to obtain material properties for failure analysis, such as fiber tensile/compressive strength, tensile and shear modulus or damage variables related to the type of loading. On the other hand, Barbero uses laminate strengths (i.e., an experimental dataset of crack densities versus applied strain or stress). It is also worth of remarking the work made by Genovese *et al.* [56], *who* developed a characterization procedure for sandwich laminates to be used on railway industry, taking into account the manufacturing process parameters. And Bruno *et al.* [57] did a review of the current optical methods used for obtain the mechanical characterization of composite materials.

The formulation used in this work, serial/parallel mixing theory, is not exonerated from requiring a similar process. The material parameters required by this formulation are those of the constituent materials. Therefore, the testing campaign should focus on obtaining such data. However, some information is difficult to obtain for the constituents themselves; for example fiber compression strength, as the material will buckle. Also, there are some material properties that are modified when the material is used as a composite constituent instead of as a bulk material, such as the effect of matrix strength in the interface area with the fiber. As a result, an adequate testing campaign to obtain the material parameters required by the formulation should look at the composite components, as well as the laminate itself.

Compared to the works described previously in which the Serial/Parallel mixing theory was used to predict a specific composite failure mode, this paper develops a methodology to obtain the material parameters required by the serial/parallel mixing theory, so it can predict all common failure modes of composites, using the same material calibration in all numerical analyses. These material parameters are obtained by means of an experimental campaign made on unidirectional laminates. To calibrate the material models, the procedure assumes that the failure of a unidirectional lamina loaded along the fiber direction is fiber-driven, while the failure of a unidirectional lamina loaded transversal to the fiber direction is assumed to be matrix-driven. Furthermore, the document describes which tests should be conducted and which material parameters are obtained from each test in order to conduct the calibration process. The described procedure, together with the formulation itself, provides a detailed methodology for the characterization of composite materials, which main advantage, compared to other existing formulations, is that it does not require to predefine the failure mode that it is expected in the composite, to predict it. Instead, the failure mode becomes part of the result given by the numerical model, and this failure mode only depends on the geometry and the loads applied to the composite. The methodology described is expected to become a guideline for future engineers that want to use S/P RoM, in order to calibrate their models for the analysis of composite structures.

In the following paragraphs, the serial-mixing theory is presented, followed by the experimental campaign designed to obtain the material data required by the formulation. The procedure developed to obtain the material parameters from the experimental data is then presented. Finally, several failure modes are simulated by the formulation and compared with the experimental results. This is done for two different composite systems, which validates the proposed methodology and formulation for obtaining the non-linear performance of composite laminates.

2. Formulation

In the present section, the numerical models that will be used to simulate composites are presented. These are based on the composite constituents. There are many models capable of simulating the elastic and specific non-linear behavior of composite laminates, as well as taking into account their anisotropic behavior. However, they are not capable of capturing different failure modes in a general way and of obtaining this failure from the failure of the composite constituents.

The formulation introduced in this work is based on the Rule of Mixtures (RoM), which obtains the composite performance by means of its constituent materials. The main advantage of the RoM versus other formulations is that once the properties of the fiber and matrix are defined, the composite response can be obtained for any fiber volumetric participation or the fiber orientation. Therefore, the necessity to test the laminate if any of these parameters are changed is suppressed.

The Rule of mixtures is based on the definition of a closing equation that relates the stresses and strains of the composite components. Depending on the relations defined, it is possible to define a direct and an inverse rule of mixtures. Both of them were originally developed by Trusdell and Toupin [45]. In order to take into account, the non-linear behavior of the composite, Oller and Car [46, 47], reformulated the classical models formulated by Trusdell and Toupin to a mechanics of the continuum media approach. Later, Rastellini [48] improved the work with the definition of a serial-parallel rule of mixtures, which can apply the direct and inverse closing equations to different directions of the strain and stress tensors.

2.1. Direct and inverse rule of mixtures

The direct rule of mixtures model is based on the following hypothesis:

i. Each infinitesimal volume of the composite contains a finite number of components.
ii. The contribution of each component to the composite behavior is proportional to its volumetric participation.
iii. The volume of each component is significantly lower than the volume of the composite.
iv. An iso-strain condition for the composite and its constituent materials is assumed in all the directions.
Next, the closing equations of the model for a composite with n constituent materials on a tensorial notation are described.
Iso-strain condition:

$$\varepsilon_c = \varepsilon_1 = \varepsilon_2 = \quad \cdots \quad = \varepsilon_n \tag{1}$$

Composite stress:

$$\sigma_c = \sum_{i=1}^{n} (V_i \cdot \sigma_i) \tag{2}$$

Assuming linear behavior of all component materials, from Equation (2), it is possible to obtain the elastic stiffness matrix of the composite:

$$^{e}C_c = \sum_{i=1}^{n} (V_i \cdot {}^{e}C_i) \tag{3}$$

A deeper understanding of these formulation can be obtained in the literature [2].
In the case of the inverse rule of mixtures, the fourth hypothesis is modified, imposing an iso-stress condition instead of an iso-strain condition. The new hypothesis reads:
v. All constituents, as well as the composite, experience the same stress (iso-stress condition).

And, therefore, the closing equations transform to Equations (4) and (5):

$$\sigma_c = \sigma_1 = \cdots = \sigma_n \tag{4}$$

$$\varepsilon_c = \sum_{i=1}^{n} (V_i \cdot \varepsilon_i) \tag{5}$$

The Elastic matrix of the composite is defined as follows:

$$\left[{}^{e}C_c\right]^{-1} = \sum_{i=1}^{n} V_i \cdot \left[{}^{e}C_i\right]^{-1} \tag{6}$$

2.2. Rule of mixtures as a constitutive law manager

In the work of Oller and Car [46, 47], the main ideas of the direct RoM theory are introduced from a thermodynamic point of view. By means of this approach, it is possible to obtain the non-linear performance of the composite if its constituents are characterized with non-linear models.

The second hypothesis (on which the mixing theory is based) states that all components contribute to the composite proportionally to their volumetric participation. Therefore, the Helmoltz free energy of the composite, ψ_c, can be obtained as the sum of the free energy of each constituent material proportional to their volumetric participation:

$$\psi_c(\varepsilon_c, \theta, \beta_c) = \sum_{i=1}^{n} V_i \cdot \psi_i(\varepsilon_i, \theta_i, \beta_i) \tag{7}$$

From the expression of the Helmotz free energy, the expression of the stress of the composite can be obtained as follows:

$$\sigma_c = \frac{\partial \psi}{\partial \varepsilon} = \sum_{i=1}^{n} V_i \cdot \frac{\partial \psi_i}{\partial \varepsilon_i} = \sum_{i=1}^{n} V_i \cdot \sigma_i \tag{8}$$

Although the equations to calculate the composite stress in the direct rule of mixture formulation, Equations (2) and (8) are the same, a big difference exists between them. Now, the RoM takes the form of a constitutive law manager, and hence, the non-linear behavior of the constituents can be taken into account. The main advantage of this strategy is that different constitutive laws can be used for the fiber and matrix. For example, the user can define the fiber as an elastic material while the matrix can be defined with an explicit damage constitutive law, resulting in a non-linear behavior of the composite.

2.3. Serial/parallel mixing theory (S/P RoM)

The S/P Mixing Theory defines two different directions in the composite, giving a more realistic performance of the laminate, capable of obtaining the anisotropic behavior of the composite. The first direction is the parallel direction, which is described along the fiber direction. The second direction is the serial direction, which encompasses all directions perpendicular and tangential to the fiber.

The formulation couples the main assumptions made by the direct and the inverse rule of mixtures, considering an iso-strain behavior in the parallel direction of the composite, while an iso-stress performance is considered in the serial direction of the composite.

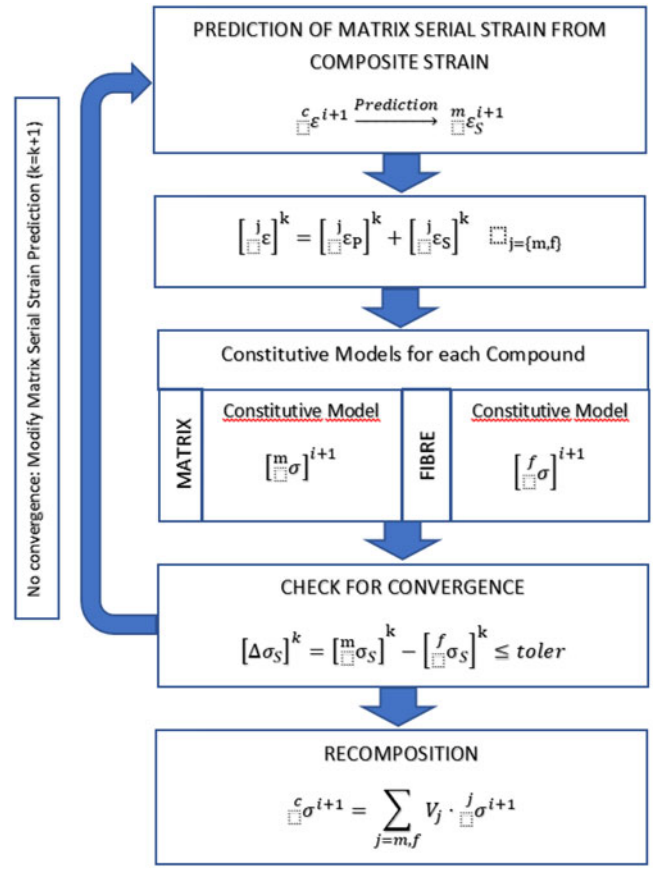

Figure 1. Flow chart of the S/P RoM algorithm.

The formulation is applied at a laminae level, allowing the definition of laminates made of several plies with a specific stacking sequence. Between the different plies of the laminate, an iso-strain condition is assumed.

The hypotheses on which this formulation is based are the following:

i. Component materials are deformed with the same strain in the fiber direction.
ii. Component materials are loaded with the same stress in all other directions.
iii. Each component contribution to the global behavior of the composite is proportional to its volumetric participation.
iv. The phases in the composite are considered homogeneously distributed.
v. Perfect physical union between components is considered.

2.3.1. S/P RoM algorithm

The proposed algorithm is a general solver for composites that uses the constitutive models of constituent materials as black boxes. This procedure allows one to use already-developed constitutive models of materials in the code. The method is defined as a strain-driven problem, because one of the material strains will be the target variable to predict. As it has been designed, the serial part of matrix strain (${}^{m}\varepsilon_S$) is selected as the independent variable of the Newton–Raphson scheme to be adopted for the algorithm.

Once the serial matrix is predicted, the fiber and matrix strains can be calculated by the independent variable and their volumetric participation on the laminate. Hence, the stress state of the constituent materials can be calculated by their constitutive models. The disequilibrium in the serial stresses between fiber and matrix ($\Delta\sigma_S = {}^m\sigma_S - {}^f\sigma_S$) is taken as the residue to be zeroed by iterative solutions. The initial prediction provides the correct strain–stress tensors for linear materials. If one of the constituent materials reaches its failure threshold, it is necessary to start an iterative process to find the strain and stress tensors for both constituents, fiber and matrix, that fulfill the closing equations.

The algorithm followed by the serial/parallel mixing theory is shown in Figure 1. For a comprehensive explanation of the algorithm, the authors suggest referring to reference [48].

2.3.2. Tangent constitutive tensor

In a non-linear analysis, the tangent stiffness tensor is required to obtain the Jacobian of the structural problem, required by a Newton–Raphson solution approach. The more accurate the determination of this tensor, the better will be the convergence of the non-linear problem.

The tangent constitutive tensor depends on the yield surface used to model each material, which implies that obtaining an analytical expression for it can be in most cases very difficult, or even impossible. With this aim, a numerical procedure to obtain the tangent constitutive tensor that can be used for any constitutive law is applied. This procedure is based on performing a numerical derivation using a perturbation method. A comprehensive description of this method can be seen in Martinez *et al.* [58].

3. Experimental campaign

In the following section, we describe the experimental campaign developed to characterize the linear and non-linear performance of composite materials. This campaign was designed to provide adequate composite material experimental data to allow a valid calibration of the Serial–Parallel mixing theory.

The tests have been conducted using two different unidirectional (UD) composite laminates: glass/epoxy (SR1125 resin from Sicomin) and glass/vinylester (LEO Injection Resin 8500 from BÜFA; this resin is part of the Saertex LEO® fire retardant composite system).

The reinforcement fabrics used in this study were SAERTEX U-E-996 g/m^2 unidirectional (UD) non-crimp glass fabric and SAERTEX U-E-940 g/m^2-LEO UD non-crimp glass fabric. The latter was used only with the LEO vinylester resin, as it is part of the LEO® composite system.

All laminates were manufactured using vacuum-assisted resin transfer molding (VaRTM) on a glass tool with a flexible membrane forming the second mold face. Laminates were manufactured using a $[0°]_{2S}$ stacking sequence. Both Sicomin and LEO resin systems were infused at ambient temperature (approximately 20 °C), following the manufacturers' instructions with respect to ratios of curing agent, curing and post-curing conditions. Test coupons were extracted using a water-cooled diamond-coated rotating disc cutter.

The following tests were conducted:

3.1. Fiber Content

Fiber content was determined using a resin burn-off method. The mass of the dry sample was recorded before and after placing the specimen in a crucible in a furnace at 550 °C for two hours. This method removes the matrix and leaves only the dry fibers behind. Where this method was not suitable, e.g., in the case of charring, thickness measurements were used to determine the fiber volume fraction.

3.2. Density

Density was determined using the water displacement method. The specimen was suspended from a support and its apparent mass when immersed in de-ionised water at 23°±2 °C was recorded. Knowing the dry mass of the specimen and the apparent mass of the support, the density of the specimen was calculated. Where this method was not suitable, e.g., the specimen mass was too low, mass and volume measurements were used to calculate the density.

3.3. Short Beam Shear Testing

Short-span three-point bend Short Beam Shear (SBS) tests were conducted under quasi-static loading conditions in accordance with ISO 14130 to determine the apparent interlaminar shear strength (ILSS). Tests were performed using a Tinius Olsen Benchtop Tester (Model 25 ST) with a 10 kN load-cell (FL04224). Nominal specimen dimensions were 30 mm x 15 mm × 3 mm. Samples were dried for 4 hours at 45 °C prior to testing. A nominal span length of 15 mm was used, at a testing speed of 1 mm/min. The upper roller diameter was 10 mm and the diameter of the lower rollers was 4 mm. Five samples were tested for each laminate. A monotonic load was applied up to the failure of each sample. A fire retardant gel coat was applied on one of the side of the SBS samples.

3.4. Flexure Testing (3-Point Bending Test)

Three-point bend tests were performed under quasi-static loading conditions. Samples were dried for 4 h at 45 °C prior to testing. The largest possible span length (80 mm) was used, at a testing speed of 1 mm/min. The upper roller diameter was 10 mm and the lower roller diameter was 4 mm. A pre-load of 20 N was applied. Sample dimensions were 200 mm × 25 mm, with a target thickness of 3 mm. Flexural strength and flexural stiffness were obtained with the fibers in the longitudinal direction and in the transverse direction were obtained. A displacement transducer (Vishay HS25) was used to measure the displacement of the sample under the load nose. Between three and six samples were

Table 1. Mechanical and physical testing results for composite laminates: ILSS and flexure (Coefficient of variation in parenthesis).

Resin class	Resin/ reinforcement	V_f (Fiber volume fraction)	Density	Apparent interlaminar shear strength	Flexural strength 0° orientation	Flexural modulus 0° orientation	Flexural strength 90° orientation	Flexural modulus 90° orientation
Vinylester	LEO SYSTEM	56%	2.233 g/cm^3	44.41 MPa	906.9 MPa	39.4 GPa	157.2 MPa	12.5 GPa
	LEO UD 940 gsm Glass	(4.3%)	(1.8%)	(8.8%)	(3.4%)	(4.6%)	(7.7%)	(5.3%)
Epoxy	SR1125	58%	2.198 g/cm^3	50.53 MPa	929.5 MPa	36.69 GPa	174.4 MPa	13.4 GPa
	UD 996 gsm Glass	(3.0%)	(2.3%)	(1.7%)	(4.6%)	(4.5%)	(3.3%)	(3.0%)

tested for each material system in each direction. The samples were tested with a monotonic load until failure.

3.5. Tensile Testing

Tensile testing was performed under quasi-static loading conditions. Samples were dried for 4 h at 45 °C prior to testing. A testing speed of 6 mm/min was used. Nominal sample dimensions were 300 mm × 25 mm × 3 mm. Tensile stiffness (Young's Modulus) was measured by loading the samples to 60% of failure. During loading, longitudinal deformation was measured using extensometers (Epsilon 3542) with a 50 mm gauge length. The sample was then unloaded, extensometers were removed and the tensile strength was established by loading the samples to failure. Tensile strength and tensile stiffness (Young's Modulus) in both the longitudinal and transverse directions were obtained. Between three and five samples where tested for each system in each direction

A summary of the results for both systems is given in Table 1 and Table 2. The load graphs of the different tests, as well as the images that show the sample failure, are included in Section 6 of this work, to facilitate the comparison of the numerical and experimental results.

4. Calibration procedure

This section describes the procedure developed to characterize the composite constituents using the results obtained in the experimental campaign detailed in the previous section. The calibration procedure proposed provides the material data, linear and non-linear, that will be assigned to the composite constituents, fiber and matrix, considering that the information obtained from the experimental campaign corresponds to a given laminae, i.e., a single layer of a long fiber-reinforced polymer.

4.1. Material parameters required by the numerical model

Some material parameters have to be introduced into the numerical model in order to obtain the composite performance. These material parameters are described in the following paragraphs.

At the laminae level, there are a number of parameters that define the configuration of the composite such as fiber orientation and fiber volume fraction. These parameters are easily obtained by testing and measuring the samples, as it has been explained in the previous section. These parameters are summarized in Table 3.

Second, one should recall that the formulation used requires the definition of a constitutive law that will be used to characterize the mechanical behavior of the composite components. Hence, the parameters that should be obtained by the calibration procedure are those required by each constitutive law considered for each constituent material. These parameters can be classified as elastic properties and failure properties.

4.1.1. Constituent properties

The relevant elastic properties are elastic modulus, Poisson coefficient and shear modulus. In the current approach, both composite constituents will be considered isotropic. However, the model is able to define anisotropic parameters, in which case it will be required to define further tests for their correct characterization.

The material non-linear properties of the constituent materials depend on the constitutive law used for their characterization. In the current work, both fiber and matrix will be analyzed with a Kachanov explicit damage law [59]. Here it must be stated that although the calibration process will be conducted for this specific constitutive model, the SP RoM can use any constitutive damage law or combination of them (i.e., a damage law for the fiber and a plastic model for the matrix). Damage in continuum solids implies a degradation of the elastic properties of the material. This process is explained by the growth of micro-cracks in the solid, reducing the effective area of the material. Hence, the solid loses its original stiffness. This phenomenon can be simulated in the context of continuum media mechanics by introducing an internal damage variable. This variable represents the degradation state of the material, relating the real stress tensor of the solid with an effective stress tensor, as it is shown in Figure 2. In the case of isotropic damage, degradation is independent of the direction, depending on a scalar parameter, d, being the relation between the real stress tensor and effective stress tensor as shown by Equation (9).

$$\boldsymbol{\sigma} = (1-d)\cdot\boldsymbol{\sigma}_0 \tag{9}$$

where $\boldsymbol{\sigma}$ is the real stress tensor of the material, $\boldsymbol{\sigma}_0$ is the effective stress tensor and d is the scalar damage variable $(0 \le d \le 1)$. Of course, the damage parameter is a measure of the loss of stiffness of the material, expressed in Equation (2).

$$\begin{aligned}\boldsymbol{\sigma} = (1-d)\cdot\boldsymbol{\sigma}_0 \rightarrow\ \ \boldsymbol{C}:\boldsymbol{\varepsilon} = (1-d)\cdot\boldsymbol{C}_0:\boldsymbol{\varepsilon} \rightarrow \boldsymbol{C} \\ = (1-d)\cdot\boldsymbol{C}_0\end{aligned} \tag{10}$$

Finally, the damage criteria distinguish between an elastic state and a damage state by comparing the stress tensor and threshold damage defined by Equation (11).

Table 2. Mechanical and physical testing results for composite laminates: tensile (Coefficient of variation in parenthesis).

Resin class	Resin/reinforcement	Tensile strength 0° orientation	Young's modulus 0° orientation	Tensile strength 90° orientation	Young's modulus 90° orientation
Vinylester	LEO SYSTEM LEO UD 940 gsm Glass	723.6 MPa (9.0%)	35.5 GPa (5.3%)	56.6 MPa (6.5%)	12.1 GPa (2.6%)
Epoxy	SR1125 UD 996 gsm Glass	855.8 MPa (5.6%)	32.4 GPa (13.6%)	66.7 MPa (3.9%)	11.0 GPa (2.1%)

Table 3. Composite parameters.

Parameter	Definition
ϑ	Fiber orientation relative to the main loading direction
V_f	Fiber volume fraction in each ply, in %.
V_{ply}	Ply volume participation on the whole composite.

$$f^D(\boldsymbol{\sigma}) - K^D(\boldsymbol{\sigma}, d) \leq 0 \tag{11}$$

Here, $f^D(\boldsymbol{\sigma})$ is the stress tensor function and $K^D(\sigma_{ij}, d)$ is the damage threshold. Its performance depends on the fracture energy of the material, G_f. The damage model allows one to use different damage threshold criteria and functions, depending on which is the real performance of the material. In this document, the damage criteria used is an exponential softening behavior, while the damage threshold function is a scalar function based on norm of principal stresses.

The material parameters required for a correct characterization of the constituents materials are listed in Table 4.

4.2. Calibration process to obtain the material parameters

This section proposes a procedure to obtain the material parameters required by the numerical model described in Section 2, using the experimental results from the tests described in Section 3. For well-known materials, most of the data required by the models can be obtained from the product datasheet. However, in many cases some parameters are unknown and, in non-common materials it will be necessary to conduct the complete experimental campaign proposed to obtain them.

Although the data required by the serial–parallel mixing theory corresponds to the composite components, the calibration procedure is defined based on an experimental campaign conducted on a unidirectional (UD) laminate. There are two main reasons to proceed in this way. The first one is the difficulty to test certain mechanical properties of the components, e.g. fiber compression strength. The second reason is related with the interaction between fibers and matrix. Many composites suppliers give a tensile strength for the neat resin higher than the transversal tensile strength of the laminate. The phenomenon is due to the interface effect between fiber and matrix, giving a poorer transversal strength to the laminate. Hence, this coupling effect should be characterized by the calibration process.

The method is based on two assumptions:

a. The longitudinal performance of the composite is driven by the fibers.
b. The transversal performance of the composite is driven by the matrix.

Hence, the fiber parameters are mainly obtained from the longitudinal tests, while the matrix parameters are obtained from the transversal tests.

4.2.1. Composite parameters

These parameters are related to the stacking sequence of the laminate and its fiber participation and usually they can be obtained from the data given by the manufacturer or supplier. In the case of the laminates used in this work, the manufacturer defined a main direction of the fiber fabric, and a secondary direction with much lower volume in the laminate. These secondary fibers, or transverse fibers, give some transversal stiffness to the whole laminate and hence, have to be taking into account, defining two plies, first one at zero degrees and the second ply at ninety degrees. In this document, the direction of a UD laminate is referring to the direction of the main volume of fibers defined in this paragraph.

Fiber volume is generally obtained by means of a burn off test. The influence of the fiber participation is directly related to the stiffness of the laminae and can be verified with a simple operation using the rule of mixtures, in other words, the stiffness of laminae is the sum of the volumetric contributions for each component. Fiber content in the main direction is defined as the results of the burn-off test, while the fiber content in the secondary direction has been defined by reverse engineering, in order to obtain a good approach of the transversal stiffness of the laminae. Finally, the volume participation of main and secondary ply on the whole laminate is obtained from the manufacturer datasheet.

4.2.2. Fiber parameters

Fiber parameters are obtained from tests performed on UD longitudinal laminates. The tests used are tensile and 3 point bending tests. In addition, in order to obtain good calibration parameters, two types of tensile tests have to be done: stiffness test and failure test. In the first test, the displacement of the sample is measured by means of an extensometers, obtaining more precise values of the stiffness. On the second test, the sample is loaded to failure, obtaining the maximum load. The reason why extensometers are not used on failure test is that the failure mode of the longitudinal UD laminates is explosive, which could damage the extensometers.

Fibers have been considered as isotropic materials and their stiffness has been obtained from the material datasheet and literature, for both Saertex Leo fiber and Hybon 2002 fiber [60–62]. In both cases, a Young Modulus value of 72 GPa was considered. The Poisson coefficient has been defined as 0.22 following a literature review [20]. The parameters obtained from the tests are fiber strength and

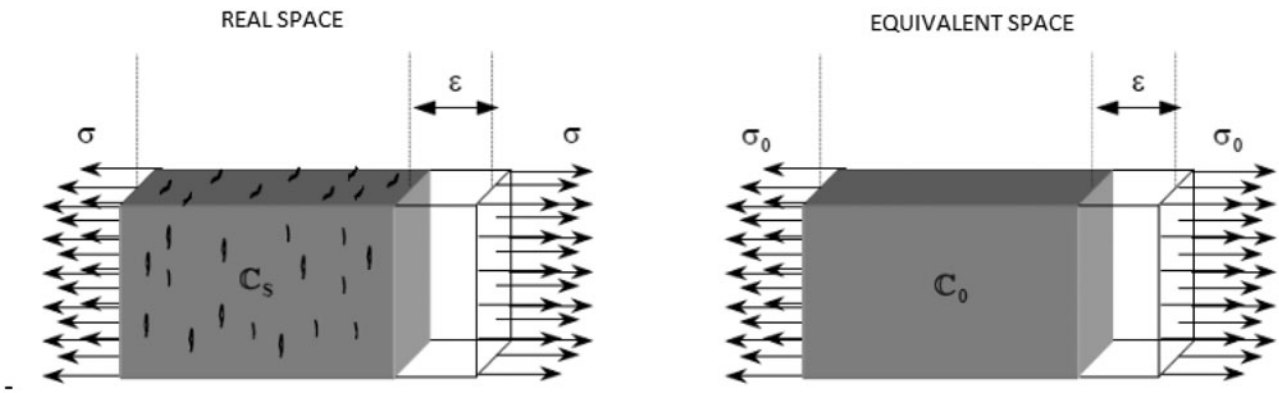

Figure 2. Representation of the effective and real stress spaces.

Table 4. Constituent material properties.

Parameter	Definition
E	Young modulus.
ν	Poisson coefficient.
G	Shear modulus.
${}^{c}\sigma_y$	Compressive strength at damage threshold.
${}^{t}\sigma_y$	Tensile strength at damage threshold
(τ_y)	Shear strength at damage threshold.
G_f	Fracture energy.
Constitutive law	Exponential softening Kachanov damage law.
Yield criteria	Norm of the principal stresses

fiber fracture energy. Fiber tensile strength was taken for the maximum load obtained in a tensile test to failure. Fiber compressive strength has been calibrated by the longitudinal bending tests, considering compressive failure of the fiber occurs when non-linear performance is reached on the load-displacement graph. Finally, the fiber energy fracture is obtained by calibration of the softening performance of the tensile test to failure.

4.2.3. Matrix parameters

Matrix parameters are obtained from tests performed on samples extracted transversally from the UD laminates. The tests used are tensile, shear and bending tests. Contrary to the longitudinal tensile tests, the failure mode of transversal tensile test is not explosive. As a consequence, extensometers could be used for both tests, i.e.. stiffness and tests to failure.

The matrix stiffness is obtained from the datasheet of the materials and from literature. The stiffness of the LEO vinylester is 3.4 GPa [20] and the stiffness of the SR1125 epoxy is 3.525 GPa [62]. For both materials, the Poisson coefficient has been defined as 0.30 [20]. Matrix tensile strength is obtained from the tensile test, considering the iso-stress condition of the S/P RoM, the transverse strength (serial performance) of the laminate is defined by the tensile strength of the first material that fails in this direction, which in the composites analyzed has been always the matrix. Matrix compression strength is obtained from the transverse flexural test, in a similar manner than the compressive strength of the fibers. The Short Beam Shear (SBS) test is used to calibrate shear stiffness and shear strength of the matrix, as well as the fracture energy of the matrix. The main reason to use the SBS test instead of tensile test to obtain the matrix fracture energy is that shear failure is matrix-dominated compared to the tensile test. Given that in transversal tensile test the UD laminate has a small percentage of fibers aligned with the loading direction, the performance is not purely matrix-dominated. Hence, the shear test is preferred to calibrate the fracture energy.

Table 5. Summary of the tests required to obtain the material parameters.

Parameter	Method to obtain
Fiber orientation	Defined by design.
Fiber and ply volume participation	Burn off test. Verified by longitudinal and transverse tensile tests.
Fiber Young modulus	Datasheet product. Verified by longitudinal tensile test.
Matrix Young modulus	Datasheet and literature. Verified by transverse tensile test.
Poisson coefficient	Literature.
Shear modulus	Short Beam Shear test (SBS).
Fiber tensile strength	Longitudinal tensile test.
Fiber compressive strength	Longitudinal 3 Point Bending Test (3PB).
Matrix tensile strength	Transverse tensile test.
Matrix compressive strength	Transverse 3PB test.
Matrix shear strength	SBS test.
Fiber fracture energy	Longitudinal tensile test.
Matrix fracture energy	SBS test.

Finally, definition of an anisotropic failure surface is necessary to properly capture the failure threshold, as tensile, compressive and shear strength differ. This can be achieved by defining a mapping between the real anisotropic space and an equivalent isotropic space, following the formulation developed by Oller [63].

4.2.4. Summary of the parameters and tests to be done

Table 5 summarizes the different parameters required by the numerical model, and the procedure used to obtain their value. Parameters are either obtained from the literature or from a specific test conducted during the experimental campaign. This table does not include as a calibration parameter the constitutive law used to simulate the material non-linear performance because, as has been stated previously, all materials have been modeled using a Kachanov damage law in the current work.

4.3. Final material parameters

The procedure described previously has been used to obtain the material parameters required to simulate the mechanical

Table 6. Summary of material properties and parameters for Leo system.

Composite properties		
Parameter	Ply 0°	Ply 90°
Ply volume	90%	10%
Fiber volume	56%	45%
Material parameters of constituent materials		
Parameter	Glass LEO fiber	LEO vinyl ester
Young modulus (GPa)	72.0	3.4
Poisson coefficient	0.22	0.30
Shear modulus (GPa)	1.66	0.455
Tensile strength (MPa)	1704	50
Compressive strength (MPa)	1500	80
Shear strength (MPa)	1704	71
Fracture energy (J/m^2)	18500	1300

Table 7. Summary of material properties and parameters for Sicomin system.

Composite properties		
Parameter	Ply 0°	Ply 90°
Ply volume	87%	13%
Fiber volume	58%	30%
Material parameters of constituent materials		
Parameter	Glass Hybon 2002	Epoxy SR1125
Young modulus (GPa)	72.0	3.525
Poisson coefficient	0.22	0.30
Shear modulus (GPa)	1.66	0.405
Tensile strength (MPa)	1707	27
Compressive strength (MPa)	1400	94
Shear strength (MPa)	1707	43
Fracture energy (J/m^2)	18500	8500

behavior of the glass/epoxy (Sicomin SR1125) and the glass/vinylester (Saertex LEO®) systems. These material parameters are displayed in Tables 6 and 7. These have been applied to the numerical models described in Section 5 to obtain the material performance that will be described in Section 6.

5. Numerical model

5.1. Geometry

The numerical models developed to calibrate the different material parameters and to reproduce the results obtained in the experimental campaign have been defined with the average dimensions obtained from the different coupons tested. These dimensions are specified in Table 8. In addition, the numerical models have been reduced to a quarter part of the entire coupon applying symmetric boundary conditions, in order to reduce the computational cost of the simulation. In the case of the longitudinal tensile test, the length used is the distance between grips, and for transverse tensile test, the distance between extensometers. Hence, the measures shown in the table correspond to the reduced model, which accounts for the applied symmetries.

For bending tests and shear tests, an elastic material on the support region has been defined in order to avoid the development of non-linear effects on these areas due to the excessive stiffness produced in numerical model by fixed supports.

Regarding meshing data, structured mesh has been defined and built with hexahedral linear elements. The meshing data for each simulation test, containing the number of nodes and elements used to create the mesh can be seen in Table 9.

The geometries of the tensile, bending and shear models for both composite systems are shown in Figures 3–5. In the case of transverse tensile tests, only the gauge length extension is defined in the FEM model.

5.2. Boundary conditions

All boundary conditions have been designed to simulate the constraints to which the specimens are subjected to. Furthermore, symmetric boundary conditions have been applied in order to reduce the number of elements used and thus the computational cost of the analysis.

Table 8. Sample dimensions.

Simulation test	Length (mm)	Width (mm)	Thickness (mm)
Tensile test	135 (50)[a]	12.5	1.5
3PB test	40	12.5	3
SBS test	7.5	7.5	3

[a]The value between parentheses corresponds to the length between extensometers for transverse tensile test model.

Table 9. Meshing data.

Simulation test	N° of elements	N° of nodes
Tensile test	20.250 (7.500)	28.184 (10.504)*
3PB test	10.000	12.636
SBS test	3.200	3.969

Values in parenthesis correspond to transverse tensile test model.

Boundary conditions for the tensile test have been applied as a null displacement and as an increasing displacement in the longitudinal direction of the sample (X direction), on surfaces defined as "X" and "D," respectively. The model is loaded with an increasing load in order to obtain a displacement-controlled performance, which allows characterizing material softening once the failure load has been reached. The symmetry boundary conditions are applied on surfaces "Y" and "Z," imposing no displacement in directions *Y* and *Z*, respectively. Figure 6, Figure 7 and Figure 8 show the surfaces in which the different boundary conditions are applied.

The flexure tests conducted on the different samples were three-point bending tests. Therefore, the sample is simply supported at both ends and a vertical displacement is applied at mid-span. These boundary conditions are applied to the numerical model by defining a null displacement at one end of the geometry (red line in Figure 7) and a continuous vertical displacement in the green surface shown in this same figure. In this last surface it is also defined a null displacement in the longitudinal direction, as it is a symmetry plane. The other symmetry plane is drawn in yellow and it is defined with a null displacement in the *Z* direction.

The same boundary conditions applied to the bending test have been applied to the Short Beam Shear test, at it is shown in Figure 8. The different behavior provided by the experimental test, as well as by the numerical model, is due to the short support span of the specimen, substantially shorter in the case of the SBS test, so the maximum stresses are tangential instead of normal.

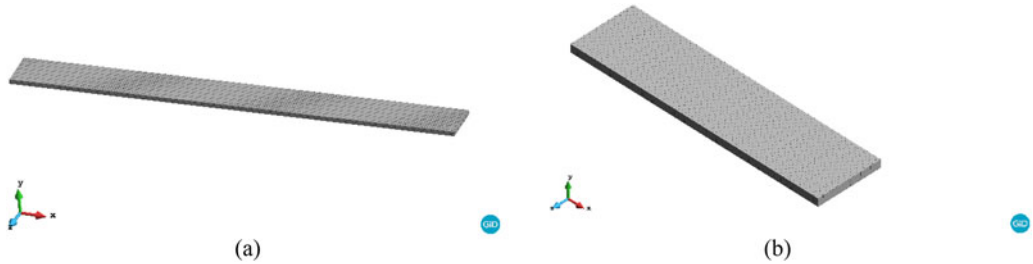

Figure 3. Geometry of the tensile test case. (a) Longitudinal tensile model. (b) Transverse tensile model.

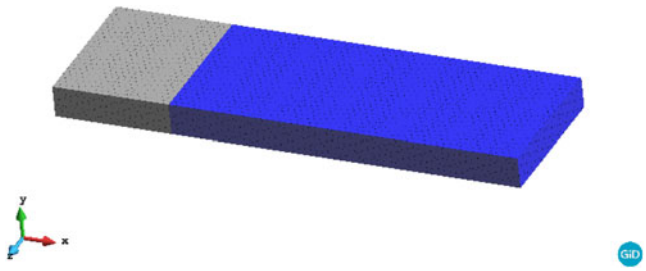

Figure 4. Geometry of the 3PB test case.

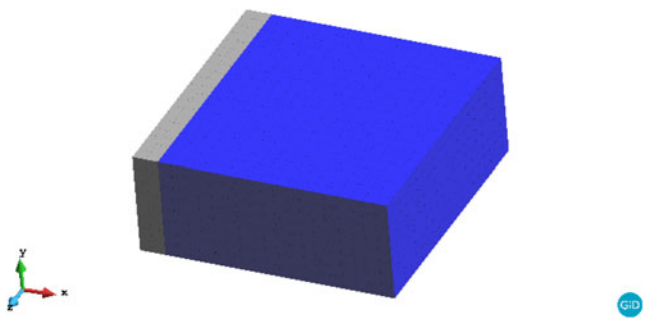

Figure 5. Geometry of the SBS test case.

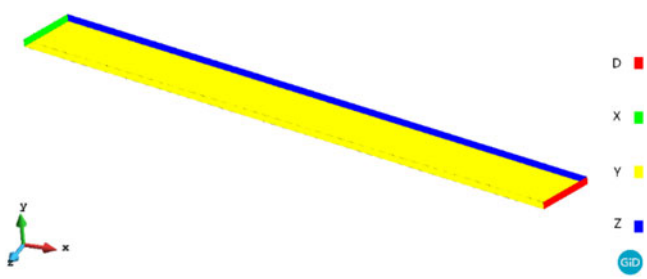

Figure 6. Boundary conditions of the tensile test.

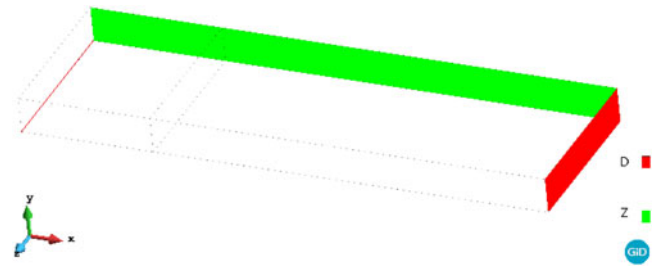

Figure 7. Boundary conditions for flexure test.

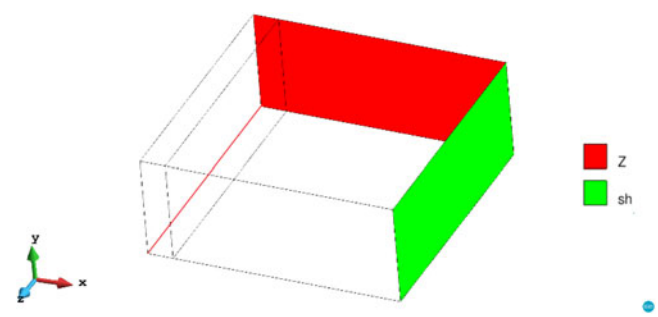

Figure 8. Boundary conditions for shear test.

6. Results and discussions

In this section, the numerical simulation results are shown and compared with the experimental results for each test and material system. The material parameters obtained by the calibration process are used to characterize the fibers and matrix of each composite system. The boundary conditions and meshing data described in previous sections have been applied. In global terms, the results show good agreement between the numerical prediction and experimental tests. The developed calibration process obtains the material parameters required by the S/P Mixing Theory. The different failure modes are obtained only changing the geometry and loading conditions of each sample. Next, the results for tensile, flexure and shear simulations, as well as their failure mode are compared to the experimental results.

6.1. Tensile tests

In terms of load–displacement, the longitudinal tensile simulations show good agreement with the experimental results. This agreement is seen in terms of stiffness and failure load of the samples. The comparison between the numerical and experimental results for load–displacement is shown in Figure 9. The results obtained on experiment samples show a generalized failure of all fibers, which is characterized as a sudden failure of the sample in an explosive manner, a very common failure mechanisms for longitudinal tensile UD laminates [64–66]. In addition, matrix failure is detected, which corresponds to the white region of the sample. These failure mechanisms can be seen on both fiber/resin systems, as it is shown in Figure 10. On the other hand, in Figure 11, the numerical results are shown. On such results, fiber damage presence exists, implying the failure of the fibers on the whole sample, as well as a high damage state on the matrix. This damage is generalized in all the sample because all of it has the same stress value. On the numerical simulation, matrix damage appears before the fiber damage, meaning

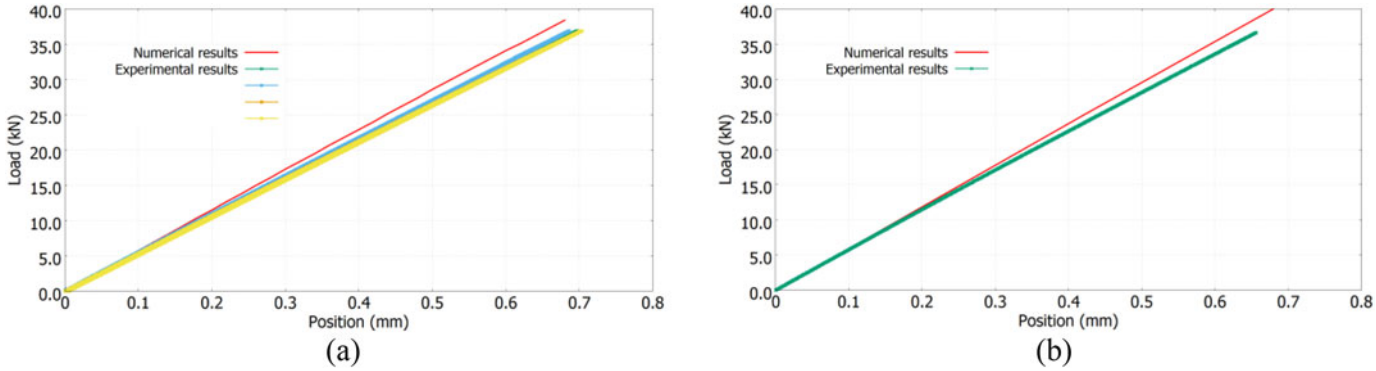

Figure 9. Longitudinal tensile stiffness results. (a) Results for LEO system. (b) Results for Sicomin system.

Figure 10. Failure mechanisms for longitudinal tensile tests. The samples show failure breakage and matrix cracking as the white region. Failure of fiber and matrix are generalized on the whole sample. For both composite systems the samples failed abruptly. (a) LEO system. (b) Sicomin system.

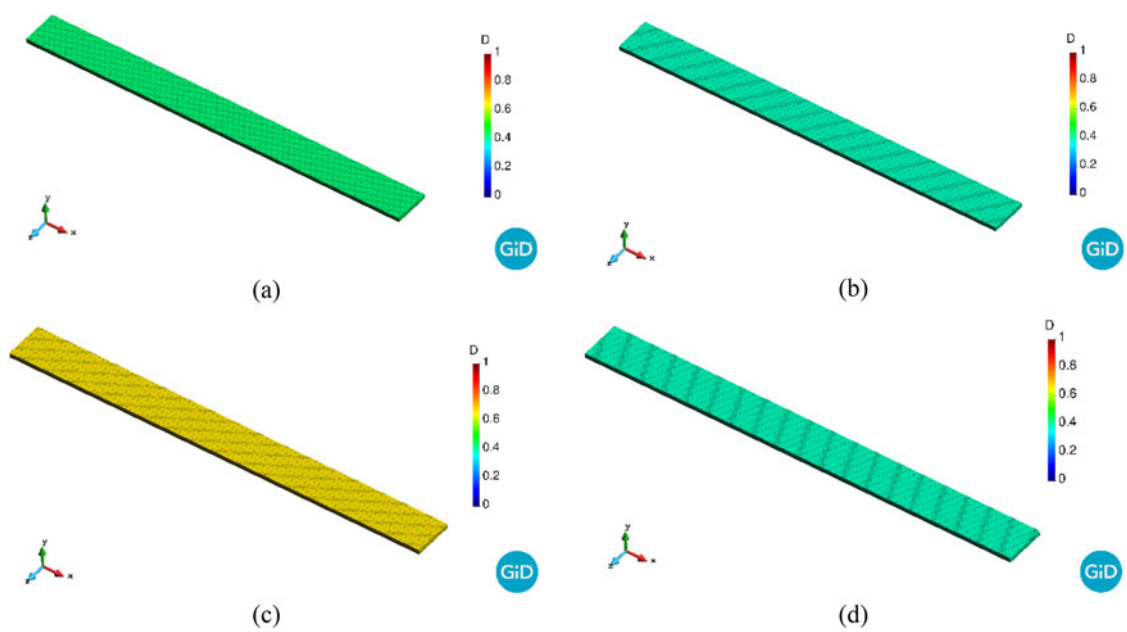

Figure 11. Numerical simulation of failure mechanisms. All pictures depict a huge extent of damage on the whole sample. (a) Fiber damage on LEO system. (b) Fiber damage on the Sicomin system. (c) Matrix damage on LEO system. (d) Matrix damage on the Sicomin system.

the apparition of matrix cracking earlier than fiber failure. Next, the initiation of fiber damage leads to the sudden drop of the load. This same process is the one that can be observed on the experimental test, proving the capability of the formulation to capture such failure mechanisms.

Load–displacement results for transverse tensile tests and their comparison with the simulations are depicted in Figure 12. In this loading condition, the primary ply of the laminate behaves on serial direction, it is an iso-stress condition, and hence the laminate has a lower stiffness and strength than a longitudinal laminate. Two linear regions for these tests are appreciated. The load at which the second linear region starts corresponds with the failure of the matrix, leading to a lower stiffness of the material. This residual stiffness, and hence residual load-bearing capacity, is believed to be given by the second ply, which in this case its fibers are parallel to the loading direction. It is important to remark that the properties of the laminate in the transverse direction are not purely matrix-dominated. Therefore, strength and stiffness in the transverse direction are higher than would be expected for pure UD fabric due to the additional properties provided by transverse fiber tows. Regarding the numerical simulations of load–displacement, it is capable to capture initial stiffness and failure load, as well as the post-failure performance. The numerical model predicts that the stiffness of this second region is probably given by the small percentage of fibers

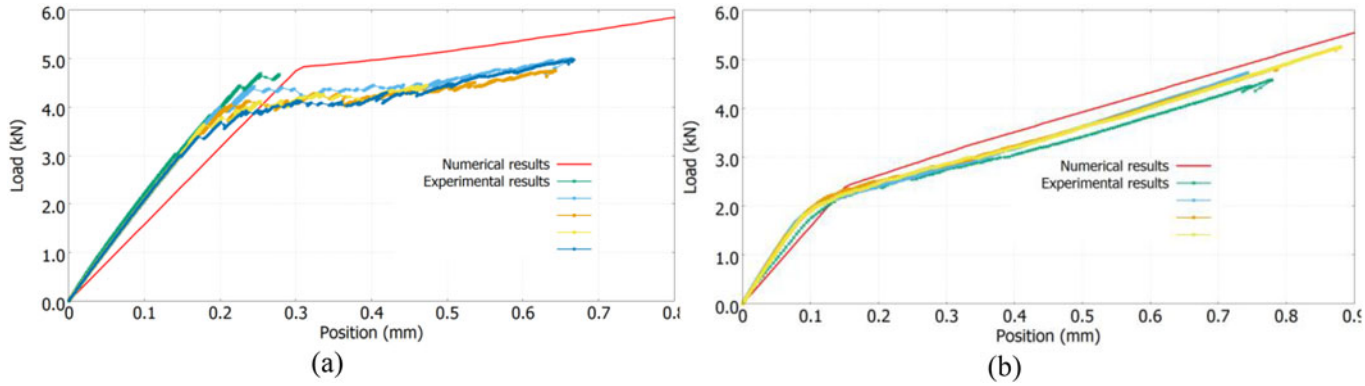

Figure 12. Load–displacement results for transverse tensile tests. (a) LEO system. (b) Sicomin system.

Figure 13. Failure mechanisms for transverse tensile tests. Both systems presented matrix failure as the white region of them. The samples did not split in two parts, given the existence of longitudinal fibers on the second ply of the laminate. (a) LEO system. (b) Sicomin system.

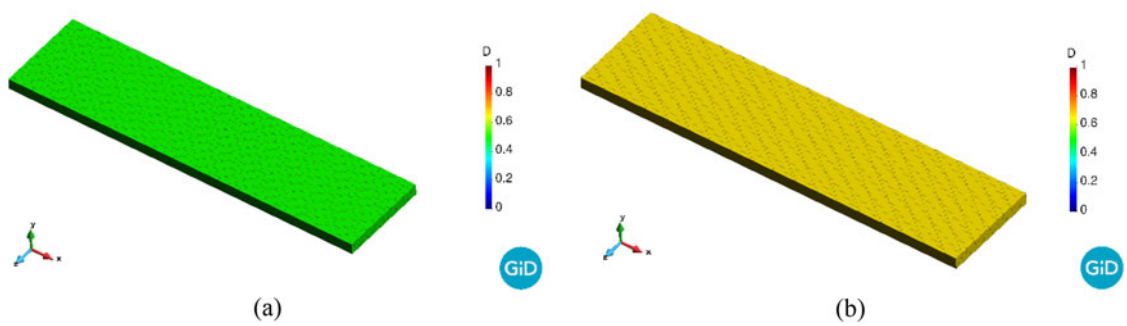

Figure 14. Numerical simulation of failure mechanisms. (a) Matrix damage for LEO system. (b) Matrix damage for Sicomin system.

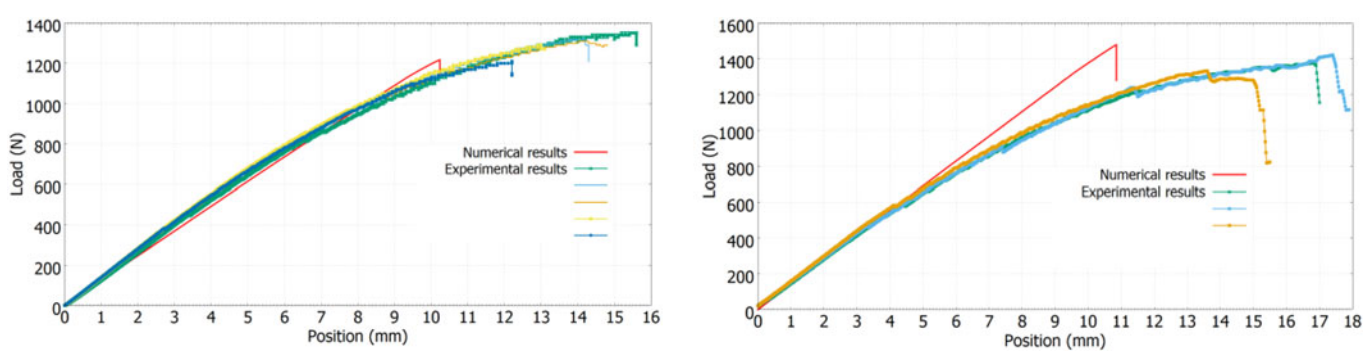

Figure 15. Load–displacement results for longitudinal 3PB tests. (a) Leo system. (b) Sicomin system.

existing the loading direction for the secondary ply of the laminate. The failure mechanism of transverse tensile test is shown in Figure 13. Although the experimental results showed some extended matrix damage on the whole samples, the failure of the matrix is clearly close to their tabs, denoted as the white region. The samples did not split in two parts and could carry some residual load. This residual load-bearing capacity was due to the second ply of the laminate, which are loaded parallel to the loading direction. The numerical results showed an extended matrix damage on the whole sample, given that all the sample is in the same stress state, as can be seen in Figure 14. Contrary on the longitudinal tests, only matrix failure appeared on transverse tensile tests, being the fibers of the second ply far from failure.

From all of the results obtained, the only numerical analysis that shows some discrepancy with the experimental results corresponds to the transversal tensile test for the LEO system. Here, the stiffness provided by the numerical model in the elastic region is somewhat smaller than the stiffness obtained experimentally. However, the failure load

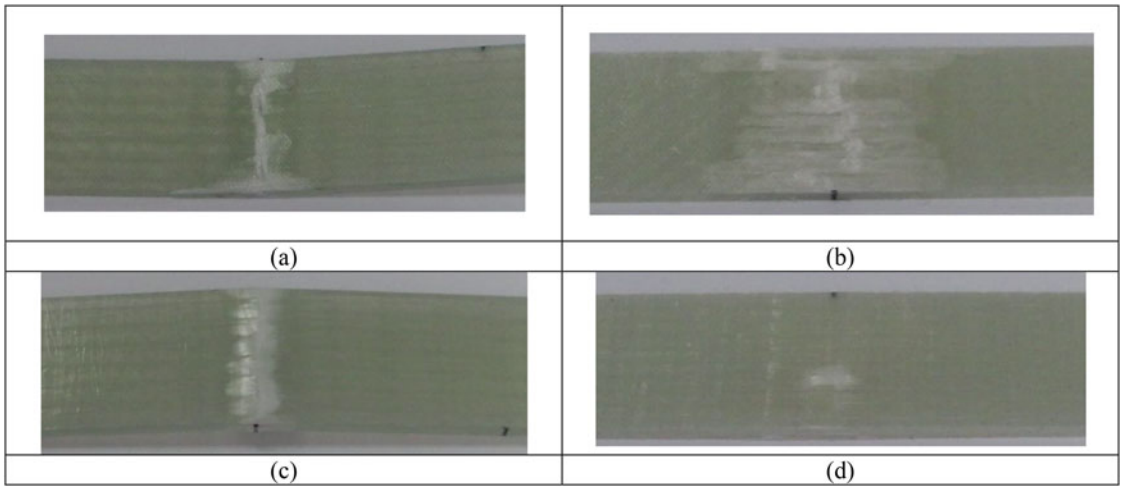

Figure 16. Failure mechanism on longitudinal 3PB tests. (a) LEO system compression side (b) Sicomin system compression side (c) LEO system tension side (d) Sicomin system tension side. LEO system exhibits a relatively narrow band of surface damage on the compression side under the load nose compared to Sicomin. Fiber bucking, delamination and matrix cracking are evident in both cases. On the tension side, 0° fiber tows are visible on LEO samples indicating fiber matrix debonding and/or delamination. Very minor damage is evident on the tension side of the Sicomin system.

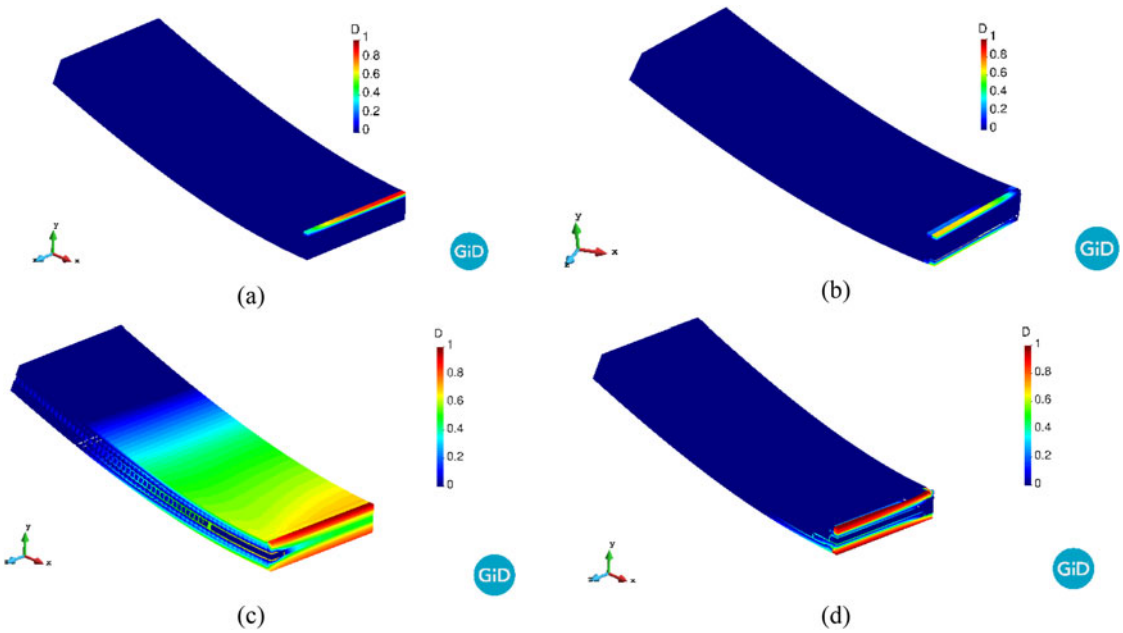

Figure 17. Numerical results for longitudinal 3PB tests. (a) Fiber damage due to compression stresses on LEO system. (b) Fiber damage mainly due to compression stresses and secondly to tensile stresses for Sicomin system. (c) Matrix damage for LEO system. Huge extension of the damage on both sides, tensile and compressive. (d) Matrix damage for Sicomin system. Larger damage extension on the tensile side.

is similar to the maximum results reported by the experimental campaign, as well as the residual stiffness of the material once matrix failure has occurred.

The tensile analysis of the composite, shown in previous figures, prove that the model is capable of providing a very good correlation of the composite stiffness. In addition, the formulation is capable of taking into account the non-linear performance of the materials, as the maximum load applied is reached as well as the composite behavior in the material non-linear range. The numerical model also provides the failure mechanisms of each simulation, which are the following: fiber breakage for longitudinal test and matrix failure for transverse test. Both numerical failures are the same obtained in the experimental campaign.

In the calibration process, some data supplied by the manufacturer were used as a first approach in the procedure and were adjusted later. Specifically, the tensile strength of the fibers used in the Sicomin system was different than the numerical value calibrated from experiments. The manufacturer specifies 2290 MPa of strength, while the tensile strength calibration is 1700 MPa. Some possible justifications that could explain this disagreement between values is the existence of a weak fiber-matrix interface, which does not allow the full development of fiber stiffness.

6.2. Flexure tests (3PB)

Load–displacement graphs for longitudinal 3PB results for both composite systems are depicted in Figure 15. Results

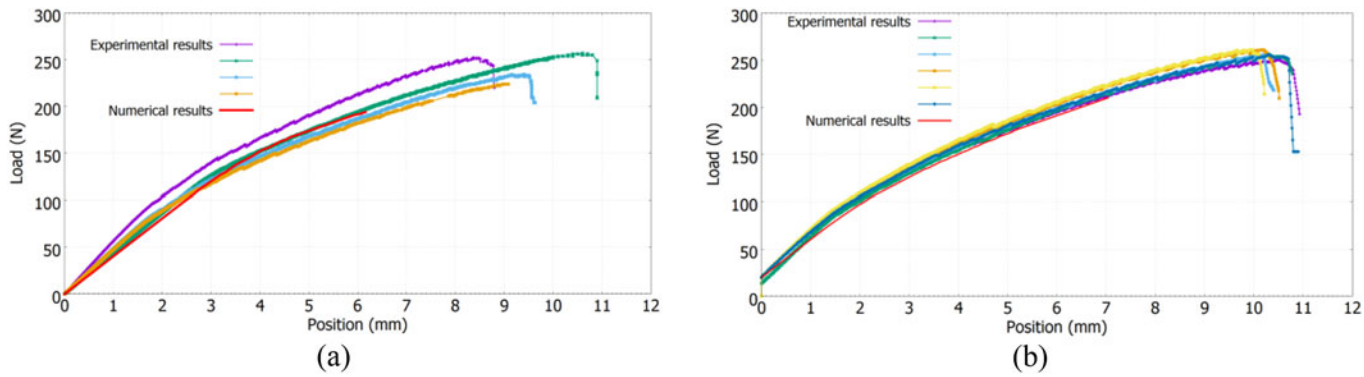

Figure 18. Load–displacement results for transverse 3PB tests. (a) LEO system. (b) Sicomin system.

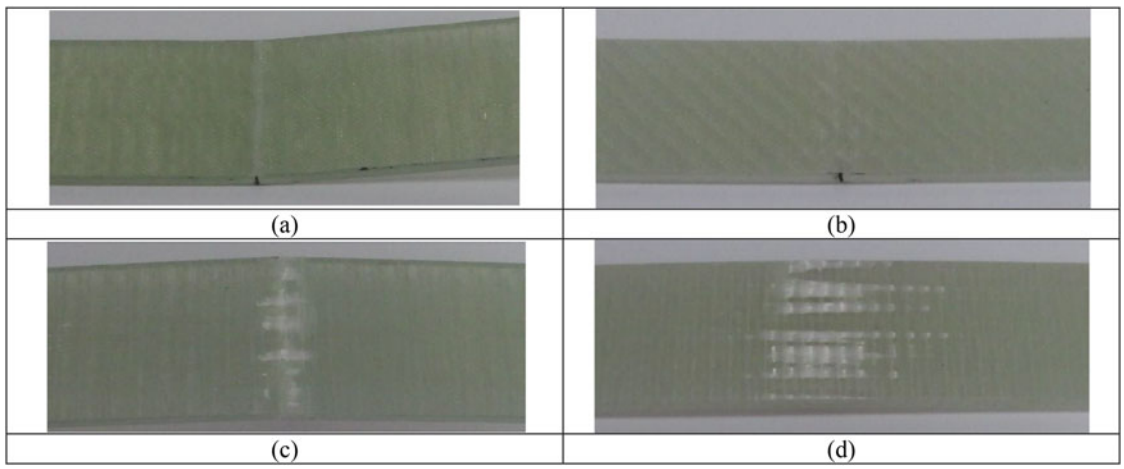

Figure 19. Experimental results for transverse 3PB tests: (a) LEO system compression side (b) Sicomin system compression side (c) LEO system tension side (d) Sicomin system tension side. A narrow band of matrix damage is evident on the compression side of both materials. Fiber tows are visible and exposed on the tension side in both samples indicating fiber-matrix debonding has occurred.

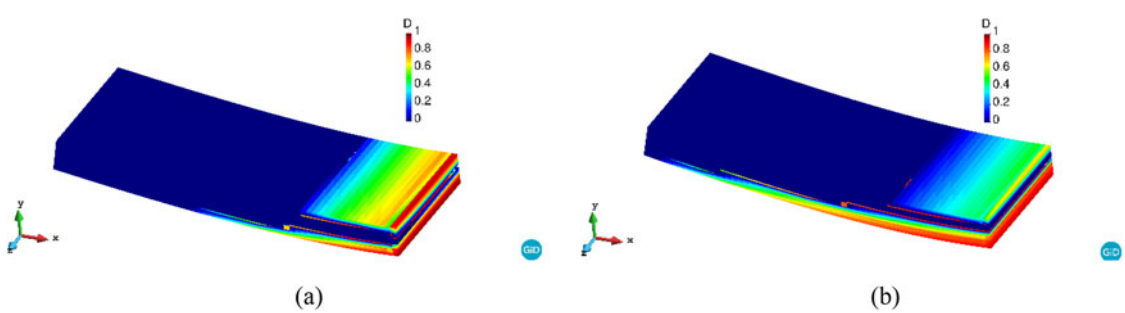

Figure 20. Numerical simulation of failure mechanisms for transverse 3PB tests. Matrix damage is depicted as the failure mechanism due to normal stresses. No fiber damage was developed. (a) LEO system. (b) Sicomin system. This system shows a larger extension of matrix damage on the tensile zone compared with LEO system.

for both composite systems show that the model is capable of capturing very accurately the bending stiffness of the composite. The numerical composite performance is mainly driven by the fiber response, which behaves linearly until failure. This differs from the response obtained experimentally, in which a gradual loss of stiffness is observed. This difference is clearly observable on the Sicomin system, as it is depicted in Figure 15 (b). However, the numerical model is capable of predicting accurately the maximum load that can be applied to each composite. In Figure 16, the results for longitudinal 3PB tests during the experimental campaign are shown. These results show that, for both composite systems, the longitudinal samples failed predominantly by fiber buckling on the compression side, although matrix damage was also observed. The compression damage in the LEO sample was narrow (concentrated under the load nose) where as a broader damage zone with obvious delamination was prevalent in the Sicomin samples. The fiber tows were visible on the tensile side of the LEO samples post-test indicating fiber-matrix debonding had occurred. Sicomin exhibited very minor damage on the tension side. Numerical predictions of failure mechanisms are shown in Figure 17. The simulations show fiber damage on the compression zone due to fiber buckling for both systems. Figure 17 (b) also shows a slight tensile fiber damage for the Sicomin system. The simulations also predict some damage in matrix

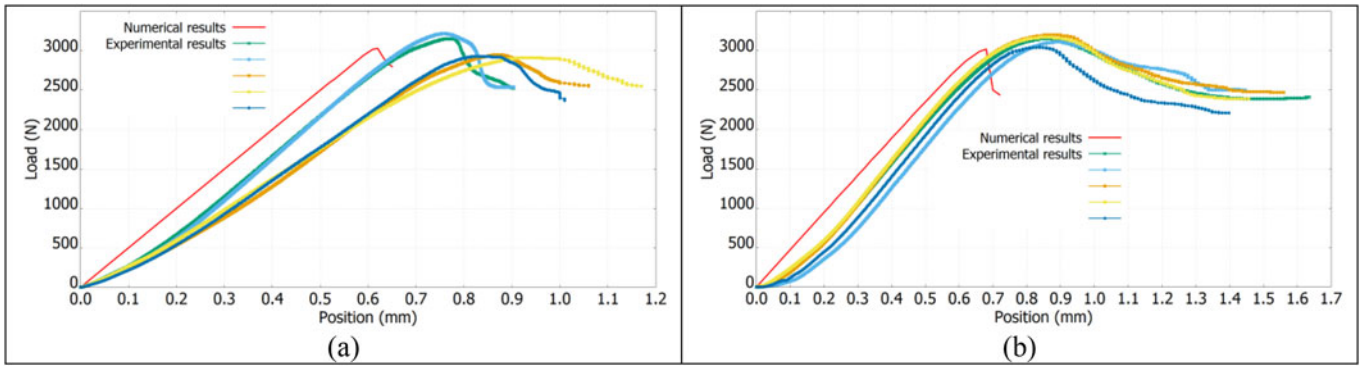

Figure 21. Load–displacement results for SBS test. (a) LEO system. (b) Sicomin system.

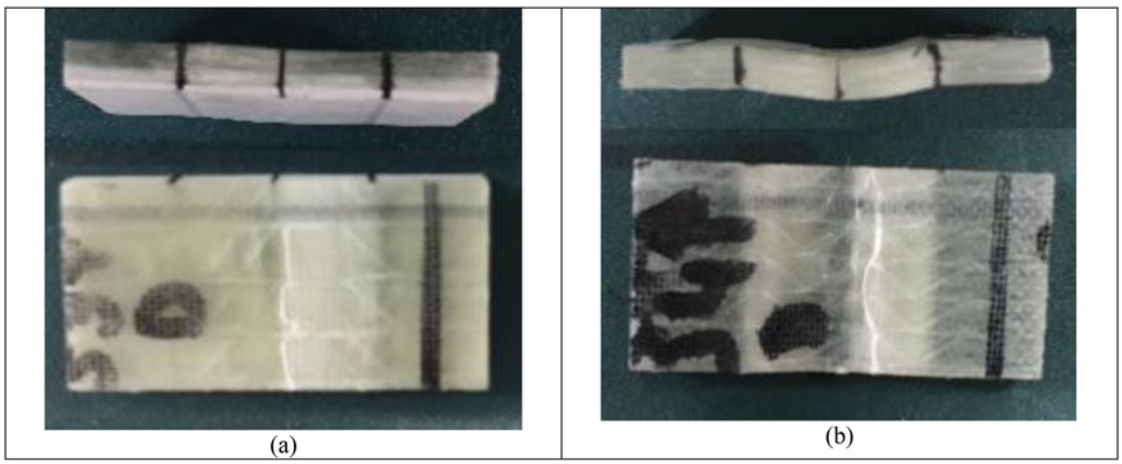

Figure 22. Failure mechanism results for SBS tests: (a) LEO system. (b) Sicomin system. In both samples, shear cracks form as white regions inside the samples between the load nose and support points.

material, which is more extended in the LEO system and can be associated to possible delaminations. The failure mode predicted by the numerical model is in agreement with the experimental failure in terms of fiber performance, as in both cases the failure is produced by fiber buckling. The numerical model is also capable of predicting the delamination in matrix material associated to the sample failure, although the model has located these delaminations in the LEO specimen, and this delamination is more extended in the Sicomin experimental sample.

The load–displacement results for transverse 3PB tests for both composite systems are shown in Figure 18. In this case, the stiffness predicted by the numerical model fits very well to the response obtained in the experimental results. This good agreement occurs in the initial linear region and also once the initial stiffness is reduced and becomes variable. However, once the non-linear regions is developed, the numerical model loses convergence before reaching the maximum load obtained in the experimental campaign. This can be explained by means of the stress concentration appeared on the mid span of the sample, where the maximum bending moment is located. In this critical section, the loss of convergence occurs in the model. On the other hand, a redistribution of stresses occurs in the experimental tests. Failure mechanisms from the experimental campaign are shown in Figure 19, where clear matrix damage is observed on both the tensile and compressive sides for both materials. Contrary to the longitudinal 3PB tests where tensile strength is higher than compressive strength due to the longitudinal fibers, the transverse 3PB are more inclined to fail in the tensile zone, given that compressive strength is higher than tensile strength for both resin systems. Fiber tows were exposed on the tensile side in both cases indicating fiber-matrix debonding had occurred. Figure 20 shows failure prediction for both composite systems, obtaining a good agreement between the experimental and numerical failure. Numerical simulations showed matrix damage as the failure mechanism. For both resin systems, tensile stresses were more critical and hence damage extension is larger in tensile side of the samples. No fiber damage was found on the numerical simulations.

6.3. Short beam shear test

The load–displacement results for the SBS simulation of both composite systems are presented in Figure 21. Shear stiffness and maximum load obtained numerically are in agreement with the experimental results for both composite systems. In both results, a clear drop in the load is observed. The load drop is as a consequence of shear crack formation, which is the main failure mechanism evident from these tests. This shear crack formation is due to the shear stress applied to the samples. Shear cracks can be seen in the tested samples shown in Figure 22, as a white region inside

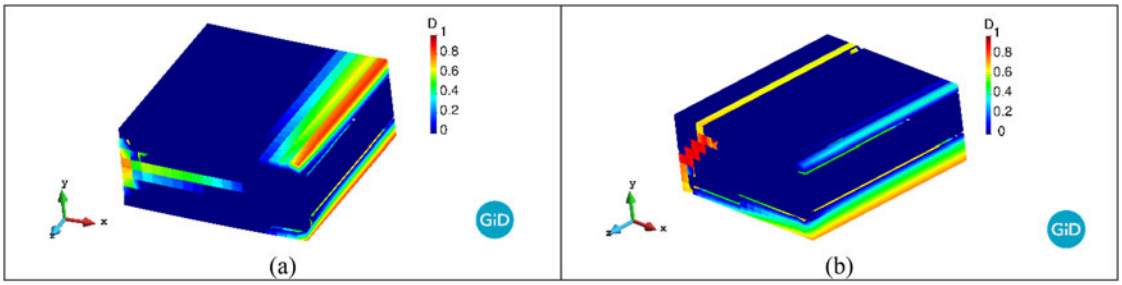

Figure 23. Numerical simulation of failure mechanisms on SBS test. Shear crack failure is observed as matrix damage on the neutral axis of the samples. In addition, tensile and compressive failure of the matrix also appears. (a) Matrix damage for LEO system. (b) Matrix damage for Sicomin system.

the thickness of the specimen. The shear bands occur between the load nose and the supports. The numerical simulations are shown in Figure 23, where matrix damage is observed on the neutral axis of the specimen, leading to shear crack failure. In addition, matrix damage due to tensile and compressive stresses is found. The damage process on the simulations is the following: matrix damage due to tensile and compressive stresses appears. Next, matrix damage initiates at the end of the specimen on the neutral axis. Finally, sudden matrix damage appears in all the neutral axis, yielding to shear cracks failure and coinciding with the drop of load on the load–displacement graph. This process is similar in both resin systems, with the exception that on the Sicomin system the shear cracks advance through the thickness until they reach the surface of the specimen. No failure of fibers was found in both composite systems.

7. Conclusions

A new methodology has been developed to obtain the material parameters required by the Serial/Parallel Mixing Theory formulation. The method uses the experimental results, obtained from the experimental analysis of unidirectional laminates, to calculate the mechanical properties of the composite constituents. The procedure assumes that failure of unidirectional laminates loaded parallel to the fiber direction is fiber-driven, while the failure of unidirectional laminates loaded off-axis is matrix-driven. The experimental campaign proposed for unidirectional laminates, the tests performed as part of the current study and the associated results are also presented.

The material parameters calculated are then used in conjunction with the Serial–Parallel Mixing Theory to predict the mechanical performance of the composites considered in this study. This formulation is capable of simulating different failure modes of the laminates, such as fiber breakage, matrix cracking and delamination, from the constitutive performance of the composite constituents. The methodology and formulation have been validated for two different composite systems, fiber-glass-reinforced vinyl ester and fiber-glass-reinforced epoxy. The results shown by the simulations prove the capacity of the model to predict the different failure mechanisms, depending on the geometry and the loads applied to the specimens, as these are the only elements that vary among the different models.

Finally, some recommendations are proposed for obtaining a good calibration process of the material parameters, which are the following:

- Stiffness measurements should be conducted with extensometers in order to obtain an accurate value of the stiffness of the material in tensile tests.
- Material parameters should be obtained from a testing campaign.
- Datasheets supplied by the manufacturers should only be used as a reference or as a first approximation of the parameters value.
- The definition of the real architecture of the laminate should be taken into account, given that it could lead to a misunderstanding of the material parameters values, as it has been proved by the need to consider the contribution of transversal fibers, included in the unidirectional laminate to stabilize the longitudinal fibers, in order to capture properly the transversal stiffness of the composite.

Up to this date, different publications had proved that the serial parallel mixing theory was an efficient method, in terms of computational cost and result accuracy, to characterize different composite failure modes. This paper has shown that with a good calibration of the composite components, the formulation is capable of predicting the most common failure modes of composites, and that the failure mode is only driven in the model by the existing stresses in the composite. This work also provides the experimental campaign and the calibration procedure required for a correct characterization of the composite components. The proven capabilities of the formulation, together with the procedure to calibrate the model, are expected to facilitate the use of this formulation for the design of optimal and reliable composite structures.

Acknowledgements

This work has been funded thanks to FibreShip Research Project, within European Union's Horizon 2020 research and innovation program under grant agreement n° 723360 "Engineering, production and life-cycle management for complete construction of large-length FIBRE-based SHIPs". http://www.fibreship.eu/about

Disclosure statement

No potential conflict of interest was reported by the authors.

References

[1] "Composite materials database available – sandia energy." [Online]. Available: https://energy.sandia.gov/latest-version-of-the-composite-materials-database-available-for-download/. Accessed: Apr 10, 2019.

[2] D. Liu, "Delamination resistance in stitched and unstitched composite plates subjected to impact loading," J. Reinf. Plast. Compos., vol. 9, no. 1, pp. 59–69, 1990. Jan. DOI: 10.1177/073168449000900104.

[3] I. Verpoest, M. Wevers, P. DeMeester, and P. Declereq, "2.5D and 3D fabrics for delamination resistant composite laminates and sandwich structure," SAMPE J., vol. 25, pp. 51–56, 1989.

[4] M. R. Wisnom and M. I. Jones, "Delamination due to interaction between overall interlaminar shear and stresses at terminating plies," Compos. Struct, vol. 31, no. 1, pp. 39–47, 1995. Jan. DOI: 10.1016/0263-8223(94)00069-7.

[5] F. W. Crossman, W. J. Warren, A. S. D. Wang, and G. E. Law, "Initiation and growth of transverse cracks and edge delamination in composite laminates Part 2. Experimental correlation," J. Compos. Mater., vol. 14, no. 1, pp. 88–108, 1980. Jan. DOI: 10.1177/002199838001400107.

[6] A. S. D. Wang and F. W. Crossman, "Initiation and growth of transverse cracks and edge delamination in composite laminates Part 1. An energy method," J. Compos. Mater, vol. 14, no. 1, pp. 71–87, Jan. 1980. DOI: 10.1177/002199838001400106.

[7] J.-L. Rebiere, "Matrix cracking and delamination evolution in composite cross-ply laminates," Cogent Eng, vol. 1, no. 1, Sep. 2014.

[8] K. Su, "Delamination resistance of stitched thermoplastic matrix composite laminates," in Advances in Thermoplastic Matrix Composite Materials. West Conshohocken, PA: ASTM International, 1989, pp. 279–300.

[9] N. S. Choi, A. J. Kinloch, and J. G. Williams, "Delamination fracture of multidirectional carbon-fiber/epoxy composites under mode I, mode II and mixed-Mode I/II loading," J. Compos. Mater, vol. 33, no. 1, pp. 73–100, 1999. Jan. DOI: 10.1177/002199839903300105.

[10] B. W. Rosen, "Tensile failure of fibrous composites," AIAA J., vol. 2, no. 11, pp. 1985–1991, 1964. Nov. DOI: 10.2514/3.2699.

[11] R. C. Sanders, E. C. Edge, and P. Grant, "Basic failure mechanisms of laminated composites and related aircraft design implications," in Composite Structures 2. Dordrecht: Springer Netherlands, 1983, pp. 467–485

[12] I. Daniel, "Failure mechanisms in fiber-reinforced composites," Proc. ARPA/AFML Rev. Prog. Quant. NDE, Sept. 1976–June 1977, May 1978.

[13] B. W. Rosen, Fiber Composite Materials: papers Presented at a Seminar of the American Society for Metals, October 17 and 18, 1964. Metals Park, OH, USA: American Society for Metals, 1965.

[14] X. Martinez, and S. Oller, "Numerical simulation of matrix reinforced composite materials subjected to compression loads," Arch. Comput. Methods Eng., vol. 16, no. 4, pp. 357–397, Dec. 2009. DOI: 10.1007/s11831-009-9036-3.

[15] H. A. Luo, and Y. Chen, "Matrix cracking in fiber-reinforced composite materials," J. Appl. Mech., vol. 58, no. 3, pp. 846 Sep. 1991. DOI: 10.1115/1.2897274.

[16] A. K. Kaw, and G. H. Besterfield, "Mechanics of multiple periodic brittle matrix cracks in unidirectional fiber-reinforced composites," Int. J. Solids Struct, vol. 29, no. 10, pp. 1193–1207, 1992. DOI: 10.1016/0020-7683(92)90231-H.

[17] R. Jamison, K. Schulte, K. Reifsnider, and W. Stinchcomb, "Characterization and analysis of damage mechanisms in tension-tension fatigue of graphite/epoxy laminates," in Effects of Defects in Composite Materials. West Conshohocken, PA: ASTM International, 1984, pp. 21–55.

[18] J. A. Nairn, "Matrix microcracking in composites," Compr. Compos. Mater, vol. 12, chap. 12, pp. 403–432, Elsevier, Jan. 2000.

[19] R. Talreja, and C. V. Singh, Damage and Failure of Composite Materials. Cambridge: Cambridge University Press, 2012.

[20] E. J. Barbero, Introduction to Composite Materials Design. 3rd edition, Taylor & Francis Group, CRC Press, Boca Raton, 2017.

[21] P. D. Soden, M. J. Hinton, and A. S. Kaddour, "A comparison of the predictive capabilities of current failure theories for composite laminates," Compos. Sci. Technol, vol. 58, no. 7, pp. 1225–1254, Jul. 1998. DOI: 10.1016/S0266-3538(98)00077-3.

[22] J. Gu, and P. Chen, "Some modifications of Hashin's failure criteria for unidirectional composite materials," Compos. Struct, vol. 182, pp. 143–152, Dec. 2017. DOI: 10.1016/j.compstruct.2017.09.011.

[23] Y. Chen *et al.*, "Yield and failure theory for unidirectional polymer-matrix composites," Compos. Part B: Eng., vol. 164, pp. 612–619, May 2019. DOI: 10.1016/j.compositesb.2019.01.071.

[24] R. Koh, and B. Madsen, "Strength failure criteria analysis for a flax fibre reinforced composite," Mech. Mater., vol. 124, pp. 26–32, 2018. Sep. DOI: 10.1016/j.mechmat.2018.05.005.

[25] P. Maimí, P. P. Camanho, J. A. Mayugo, and C. G. Dávila, "A continuum damage model for composite laminates: Part I – constitutive model," Mech. Mater, vol. 39, no. 10, pp. 897–908, Oct. 2007.

[26] P. Maimí, P. P. Camanho, J. A. Mayugo, and C. G. Dávila, "A continuum damage model for composite laminates: Part II – computational implementation and validation," Mech. Mater, vol. 39, no. 10, pp. 909–919, Oct. 2007.

[27] C. G. Davila, P. P. Camanho, and C. A. Rose, "Failure criteria for FRP laminates," J. Compos. Mater., vol. 39, no. 4, pp. 323–345, Feb. 2005. DOI: 10.1177/0021998305046452.

[28] S. T. Pinho, C. G. Dávila, P. P. Camanho, L. Iannucci, and P. Robinson, "Failure models and criteria for FRP under in-plane or three-dimensional stress states including shear non-linearity." NASA/TM-2005-213530. Available: http://www.sti.nasa.gov," 2005.

[29] E. J. Barbero, and D. H. Cortes, "A mechanistic model for transverse damage initiation, evolution, and stiffness reduction in laminated composites," Compos. Part B: Eng., vol. 41, no. 2, pp. 124–132, Mar. 2010. DOI: 10.1016/j.compositesb.2009.10.001.

[30] P. Ladevèze, O. Allix, J.-F. Deü, and D. Lévêque, "A mesomodel for localisation and damage computation in laminates," Comput. Methods Appl. Mech. Eng, vol. 183, no. 1/2, pp. 105–122, Mar. 2000. DOI: 10.1016/S0045-7825(99)00214-5.

[31] A. Matzenmiller, J. Lubliner, and R. L. Taylor, "A constitutive model for anisotropic damage in fiber-composites," Mech. Mater., vol. 20, no. 2, pp. 125–152, Apr. 1995. DOI: 10.1016/0167-6636(94)00053-0.

[32] K. V. Williams, R. Vaziri, and A. Poursartip, "A physically based continuum damage mechanics model for thin laminated composite structures," Int. J. Solids Struct., vol. 40, no. 9, pp. 2267–2300, May 2003. DOI: 10.1016/S0020-7683(03)00016-7.

[33] E. Barbero, and P. Lonetti, "Damage model for composites defined in terms of available data," Mech. Adv. Mat. Struct., vol. 8, no. 4, pp. 299–315, Oct. 2001. DOI: 10.1080/107594101753172539.

[34] E. J. Barbero, G. F. Abdelal, and A. Caceres, "A micromechanics approach for damage modeling of polymer matrix composites," Compos. Struct, vol. 67, no. 4, pp. 427–436, Mar. 2005. DOI: 10.1016/j.compstruct.2004.02.001.

[35] S. P. H. Skovsgaard, and H. M. Jensen, "Three-dimensional constitutive model for elastic-plastic behaviour of fibre-reinforced composites," Int. J. Solids Struct., vol. 139–140, pp. 150–162, May 2018. DOI: 10.1016/j.ijsolstr.2018.01.032.

[36] S. P. H. Skovsgaard, and H. M. Jensen, "Constitutive model for imperfectly bonded fibre-reinforced composites," Compos. Struct, vol. 192, pp. 82–92, May 2018. DOI: 10.1016/j.compstruct.2018.02.053.

[37] D. J. O'Shea, M. M. Attard, and D. C. Kellermann, "Hyperelastic constitutive modelling for transversely isotropic composites and orthotropic biological tissues," Int. J. Solids

Struct., vol. 169, pp. 1–20, Sep. 2019. DOI: 10.1016/j.ijsolstr.2018.07.013.

[38] B. Staber, J. Guilleminot, C. Soize, J. Michopoulos, and A. Iliopoulos, "Stochastic modeling and identification of a hyperelastic constitutive model for laminated composites," Comput. Methods Appl. Mech. Eng., vol. 347, pp. 425–444, Apr. 2019. DOI: 10.1016/j.cma.2018.12.036.

[39] F. Otero, S. Oller, and X. Martinez, "Multiscale computational homogenization: review and proposal of a new enhanced-first-order method," Arch. Comput. Methods Eng., vol. 25, no. 2, pp. 479–505, Apr. 2018. DOI: 10.1007/s11831-016-9205-0.

[40] Y. Chen, Z. Guo, X.-L. Gao, L. Dong, and Z. Zhong, "Constitutive modeling of viscoelastic fiber-reinforced composites at finite deformations," Mech. Mater, vol. 131, pp. 102–112, Apr. 2019. DOI: 10.1016/j.mechmat.2019.02.001.

[41] X. Liu, W. Yu, F. Gasco, and J. Goodsell, "A unified approach for thermoelastic constitutive modeling of composite structures," Compos. Part B Eng, vol. 172, pp. 649–659, Sep. 2019. DOI: 10.1016/j.compositesb.2019.05.083.

[42] F. Otero, S. Oller, X. Martinez, and O. Salomón, "Numerical homogenization for composite materials analysis. Comparison with other micro mechanical formulations," Compos. Struct., vol. 122, pp. 405–416, Apr. 2015. DOI: 10.1016/j.compstruct.2014.11.041.

[43] F. Otero, X. Martinez, S. Oller, and O. Salomón, "An efficient multi-scale method for non-linear analysis of composite structures," Compos. Struct., vol. 131, pp. 707–719, Nov. 2015. DOI: 10.1016/j.compstruct.2015.06.006.

[44] S. Zaghi, X. Martinez, R. Rossi, and M. Petracca, "Adaptive and off-line techniques for non-linear multiscale analysis," Compos. Struct., vol. 206, pp. 215–233, Dec. 2018. DOI: 10.1016/j.compstruct.2018.08.022.

[45] C. Truesdell and R. Toupin, The Classical Field Theories. Springer, Berlin, Heidelberg, 1960, pp. 226–858.

[46] E. Car, S. Oller, and E. Oñate, "An anisotropic elastoplastic constitutive model for large strain analysis of fiber reinforced composite materials," Comput. Methods Appl. Mech. Eng., vol. 185, no. 2-4, pp. 245–277, May 2000. DOI: 10.1016/S0045-7825(99)00262-5.

[47] E. Car, F. Zalamea, S. Oller, J. Miquel, and E. Oñate, "Numerical simulation of fiber reinforced composite materials––two procedures," Int. J. Solids Struct., vol. 39, no. 7, pp. 1967–1986, Apr. 2002. DOI: 10.1016/S0020-7683(01)00240-2.

[48] F. Rastellini, S. Oller, O. Salomón, and E. Oñate, "Composite materials non-linear modelling for long fibre-reinforced laminates: Continuum basis, computational aspects and validations," Comput. Struct., vol. 86, no. 9, pp. 879–896, May 2008. DOI: 10.1016/j.compstruc.2007.04.009.

[49] X. Martínez, S. Oller, and E. Barbero, Study of Delamination in Composites by Using the Serial/Parallel Mixing Theory and a Damage Formulation. Dordrecht: Springer, 2008, pp. 119–140.

[50] X. Martinez, F. Rastellini, S. Oller, F. Flores, and E. Oñate, "Computationally optimized formulation for the simulation of composite materials and delamination failures," Compos. Part B: Eng., vol. 42, no. 2, pp. 134–144, Mar. 2011. DOI: 10.1016/j.compositesb.2010.09.013.

[51] M. A. Pérez, X. Martínez, S. Oller, L. Gil, F. Rastellini, and F. Flores, "Impact damage prediction in carbon fiber-reinforced laminated composite using the matrix-reinforced mixing theory," Compos. Struct., vol. 104, pp. 239–248, Oct. 2013. DOI: 10.1016/j.compstruct.2013.04.021.

[52] A. Solis, S. Sanchez-Saez, X. Martinez, and E. Barbero-Pozuelo, "Numerical analysis of interlaminar stresses in open-hole laminates under compression," Compos. Struct., vol. 217, pp. 89–99, Jun. 2019. DOI: 10.1016/j.compstruct.2019.03.027.

[53] M. L. Ribeiro, V. Tita, and D. Vandepitte, "A new damage model for composite laminates," Compos. Struct., vol. 94, no. 2, pp. 635–642, Jan. 2012. DOI: 10.1016/j.compstruct.2011.08.031.

[54] E. J. Barbero, F. A. Cosso, R. Roman, and T. L. Weadon, "Determination of material parameters for Abaqus progressive damage analysis of E-glass epoxy laminates," Compos. Part B: Eng., vol. 46, pp. 211–220, Mar. 2013. DOI: 10.1016/j.compositesb.2012.09.069.

[55] E. J. Barbero, and J. C. Barbero, "Determination of material properties for progressive damage analysis of carbon/epoxy laminates," Mech. Adv. Mater. Struct., vol. 26, no. 11, pp. 938–947, 2019.

[56] A. Genovese, M. Russo, and S. Strano, "Mechanical characterization and modeling of an innovative composite material for railway applications," Proc. Inst. Mech. Eng. Part L J. Mater. Des. Appl., vol. 231, no. 1/2, pp. 122–130, Feb. 2017. DOI: 10.1177/1464420716665648.

[57] L. Bruno, "Mechanical characterization of composite materials by optical techniques: A review," Opt. Lasers Eng., vol. 104, pp. 192–203, May 2018. DOI: 10.1016/j.optlaseng.2017.06.016.

[58] X. Martinez, S. Oller, F. Rastellini, and A. H. Barbat, "A numerical procedure simulating RC structures reinforced with FRP using the serial/parallel mixing theory," Comput. Struct, vol. 86, no. 15/16, pp. 1604–1618, Aug. 2008. DOI: 10.1016/j.compstruc.2008.01.007.

[59] S. Oller, Nonlinear Dynamics of Structures. Cham: Springer International Publishing, 2014.

[60] "SAERTEX-LEO® fire protection meets new safety standards." [Online]. Available: https://www.saertex.com/en/support/press-service/p-span-lang-en-gb-strong-saertex-strong-leo-sup-sup-combines-high-mechanical-performance-with-fire-safety-and-environmental-protection-requirements-span-p. Accessed: Apr 10, 2019.

[61] "HYBON® 2002 - PPG Industries - datasheet." [Online]. Available: https://polymer-additives.specialchem.com/product/a-ppg-industries-hybon-2002. Accessed: Apr 12, 2019.

[62] "Sicomin Epoxy Systems And Composite Materials." [Online]. Available: http://www.sicomin.com/. Accessed: Apr 12, 2019.

[63] S. Oller, Numerical Simulation of Mechanical Behavior of Composite Materials. first. Cham: Springer International Publishing, 2014.

[64] V. M. Harik, J. R. Klinger, and T. A. Bogetti, "Low Cycle Fatigue of Unidirectional Laminates: Stress Ratio Effects," J. Eng. Mater. Technol., vol. 122, no. 4, pp. 415, Oct. 2000. DOI: 10.1115/1.1289024.

[65] Y. Ma, Y. Yang, T. Sugahara, and H. Hamada, "A study on the failure behavior and mechanical properties of unidirectional fiber reinforced thermosetting and thermoplastic composites," Compos. Part B Eng., vol. 99, pp. 162–172, 2016. Aug. DOI: 10.1016/j.compositesb.2016.06.005.

[66] M. M. Tahir, W.-X. Wang, and T. Matsubara, "A novel tab for tensile testing of unidirectional thermoplastic composites," J. Thermoplast. Compos. Mater., vol. 32, no. 1, pp. 37–51, 2019. Jan. DOI: 10.1177/0892705717743295.